Imperial College London

Imperial College London

Department of Aeronautics

Semi-Empirical Optimisation of the Shape of a Surface Reducing Turbulent Skin Friction

Author:

Herman (Hon Man) Mak

Supervisor:

Prof. Sergei Chernyshenko

Submitted in partial fulfilment of the requirements for the degree of

MSc Advanced Aeronautical Engineering

September, 2021

Abstract

Your abstract goes here. The abstract is a very brief summary of the dissertation's contents. It should be about half a page long. Somebody unfamiliar with your project should have a good idea of what it's about having read the abstract alone and will know whether it will be of interest to them.

Acknowledgements

It is usual to thank those individuals who have provided particularly useful assistance, technical or otherwise, during your project.

Contents

List of Figures

Acronyms

BL boundary layer.

CFD computational fluid dynamics.

DNS direct numerical simulation.

DR drag reduction.

ODE ordinary differential equation.

PDE partial differential equation.

RANS Reynolds Averaged Navier-Stokes.

SSL spatial Stokes layer.

TBL turbulent boundary layer.

TRL technology readiness level.

TSL temporal Stokes layer.

WW wavy wall.

Notation

A oscillation amplitude of spanwise wall velocity W_w (sometimes denoted A_{ssl}).

A_g^+ riblet groove area in wall units.

A_w wavy wall oscillation amplitude (sometimes denoted α).

B a constant in the logarithmic profile $\frac{1}{\kappa} \ln y^+ + B + \Delta h$, it is equal to 5.0.

Δh the vertical increase in the logarithmic profile accompanying drag reduction $\frac{1}{\kappa} \ln y^+ + B + \Delta h$.

h channel half height.

k wavenumber $k = \frac{2\pi}{\lambda}$ (any subscript denotes direction).

p pressure field, it is equal to its triple decomposition, which is $\overline{P} + \tilde{p} + p'$.

$\overline{p}$ mean pressure.

$\tilde{p}$ periodically fluctuating pressure field.

p' randomly fluctuating pressure field.

$\boldsymbol{Re}$ Reynolds number, and is equal to $\frac{UL}{\nu}$, a characteristic velocity U multiplied by a characteristic length L divided by kinematic viscosity ν.

$\boldsymbol{Re}_\tau$ friction Reynolds number, defined using friction velocity u_τ and channel half height h as the characteristic velocity and length respectively.

$\mathbf{s}$ denoting the spatial Stokes layer (SSL) flow.

t time.

T oscillation period.

$\mathbf{U}$ velocity vector with components (U, V, W), the triple decomposition thereof is $\mathbf{U} = \overline{\mathbf{U}} + \tilde{\mathbf{u}} + \mathbf{u}'$.

U x component of velocity (similarly V, W are the y, z components of velocity respectively).

$\overline{\mathbf{U}}$ mean velocity vector with components $(\overline{U}, \overline{V}, \overline{W})$.

$\tilde{\mathbf{u}}$ phase averaged velocity vector with components $(\tilde{u}, \tilde{v}, \tilde{w})$.

$\mathbf{u}'$ randomly fluctuating velocity vector with components (u', v', w').

$\breve{u}^+$ part of phase average velocity in the x direction dependent on $\breve{y}^+$.

$\hat{U}$ amplitude of the phase average oscillation in the x direction $\tilde{U}$.

u_τ friction wall velocity; it is equal to $\sqrt{\frac{\tau_w}{\rho}}$.

$\mathbf{w}$ denoting the oblique wavy wall (WW) flow (note different from w, which denotes the variable is measured at the wall).

$\breve{w}^+$ part of phase average velocity in the z direction dependent on $\breve{y}^+$.

$\hat{W}$ amplitude of the phase average oscillation in the z direction $\tilde{W}$.

W_w spanwise wall velocity.

$\breve{y}^+$ equal to $(k_x^+)^{-1/3} y^+$.

$y_\times^+$ the crossing point between the linear profile $\overline{U}^+ = y^+$ and the logarithmic profile $\frac{1}{\kappa} \ln y^+ + B + \Delta h$.

$\mathbf{0}$ denoting the reference channel flow.

α amplitude of the height of undulations of the wavy wall.

κ a constant in the logarithmic profile $\frac{1}{\kappa} \ln y^+ + B + \Delta h$, it is equal to 0.41.

λ wavelength (any subscript denotes direction).

μ dynamic viscosity.

ν kinematic viscosity, defined as the ratio between dynamic viscosity and density $\frac{\mu}{\rho}$.

ϕ phase along a wave or phase shift for WW.

Φ dissipation rate per unit area.

ρ fluid density.

τ_w wall shear stress.

θ oblique angle between wavy wall and streamwise direction.

Chapter 1

Introduction

1.1 Motivation

Whether it be water in a pipeline, or an aircraft soaring through the skies, every fluid passing by a solid and every solid passing through a fluid will experience drag. The ever pressing need to reduce our impact on the environment requires us to reduce our energy used to combat unwanted drag, which also has the added benefit of reducing costs via increased efficiency. This is especially true in the transportation sector, which accounts for 24% of total global emissions in 2019 according to the IEA, although growth has been limited to only 0.5% per year compared to an average increase of 1.9% annually since 2000 owing to efficiency improvements [1].

The search for these efficiency improvements includes research towards drag reduction (DR) via flow control – that is manipulating the flow characteristics in such a way that somehow produces less overall drag. In fact, Ludwig Prandtl, who revolutionised the study of fluid mechanics with the introduction of the turbulent boundary layer (TBL), pioneered modern flow control as early as 1904, where he demonstrated that suction at the surface of a cylinder delays boundary layer (BL) separation and therefore decreases drag [2, 3]. Indeed, DR is a major focus of research in commercial aviation. In the context of aviation, a 1% reduction in drag corresponds to a 0.75% reduction in fuel and as a result CO_2 emissions [4]. In fact, [4] states that based on estimates on travel demand in 2030, a 1% reduction will constitute a 9 million tonnes reduction in CO_2 emissions.

In transport applications, and in particular aviation, the flows are at high Reynolds numbers Re, this means the regimes we are dealing with are often turbulent. Moreover, especially in aviation (with the exception of cases where supersonic effects dominate), viscous drag generated in the near-wall BL region constitutes a major component of total drag [5]. These two factors combined mean that "flow control methodology targeting the TBL is the most obvious option to achieve a significant skin-friction-drag reduction and ultimately to reduce emissions" [5].

Flow control is separated into two distinct groups, active and passive control. Active flow control requires an input in energy to affect the flow via the use of actuators, whereas passive

flow control does not. Examples of active control include opposition control [6, 7], spanwise-wall oscillation [8–10], and the aforementioned BL separation control [3]; the former is closed-loop and reacts to sensor inputs from the environment, whereas the latter two can be either open-loop with predetermined control patterns or reactive (feedback/feed-forward systems). The actuators used to perform active flow control can range from zero-net-mass-flux jets [11], to dielectric-barrier-discharge plasma actuators [12], to fluid injection (blowing) and sucking [13], to the ingenious moving surface using "pneumatically actuated compliant structure based on the kagome lattice geometry" [14]. Whereas, examples of passive control include vortex generators [15], discontinuities/notches/fences in the leading/rear edges of a wing [15], compliant surfaces [16], porous coatings [17], superhydrophobic surfaces [18], and a very well studied control technique known as riblets [19–21].

As aforementioned, active flow control allows for reactive responses which can increase the effectiveness of control techniques. Moreover, even open-loop flow control can achieve higher viscous drag reduction than passive control techniques without the need for sensors required for reactive flow control. However, this comes at a cost of the extra energy expended to modify the flow and the difficulty and innovation needed to design actuators. This can clearly be seen in the case of spanwise-wall oscillation where the wall moves as prescribed by a streamwise travelling wave, which, after accounting for the power spent to oscillate the fluid, has a net power saving of around 26% despite a drag reduction of $> 35\%$ for those conditions [22]. Moreover, in order to emulate a in-plane wall motion in real life, the aforementioned compliant structure from [14] had to be created and trialled in laboratory conditions, and then made at scale and maintained if it were to be used on real-world flows.

On the other hand, passive flow control in necessarily open-loop, and may have decreased performance in comparison to active flow control. However, it does not require actuators and the maintenance thereof. Riblets, for example, "are small surface protrusions aligned with the direction of the flow, which confer an anisotropic roughness to a surface" [21] and can be seen in Figure 1.1. Experiments show that under moderate adverse pressure gradient (i.e. where the pressure increases along the direction of the flow) a 13% skin friction reduction is achievable, compared to 6% reduction in a zero-pressure-gradient BL [23]. Although less efficient compared to active control, due to its relatively simple design, its technology readiness level (TRL) is higher than most other flow control techniques. In fact it has been trialled in scale model aircraft tests in transonic Mach numbers [24], real aircraft tests, and even in commercial service for several years by Cathay Pacific on an Airbus A340 where 30% of the wetted surface was covered with riblets [25]. Based on a flight test on an Airbus A320, in transonic Mach number ranges, an A320 with 70% of the wetted surface covered by riblets could have a drag reduction of about 2% [26]. However, the optimal grove cross section was found to have an optimum at $\left(A_g^+\right)^{1/2} \approx 11$, where the $+$ superscript denotes non-dimensionalisation by wall units (see 1.2.1) and spacing of approximately 15 wall units [21]. This is equivalent to approximately 30–70 µm in realistic aerofoil and aircraft flows [21]. Moreover, the sharper the riblets, the more efficient they are at reducing drag [21]. All

of these factors make riblets quite hard to manufacture whilst requiring maintenance/replacements due to the erosion from air moving past.
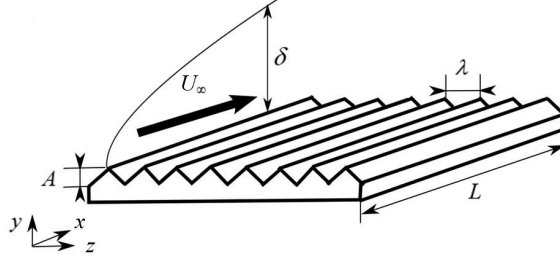

Figure 1.1: A schematic of triangular riblets; the most commonly researched riblets. Figure modified from [27].

Therefore, researchers have begun to explore other ways to use passive flow control for turbulent DR. The oblique wavy wall (WW) was first proposed by Chernyshenko [28] in 2013 to emulate the motions of in-plane spanwise wall oscillations in hopes that there will be a net energy decrease. We will devote the rest of this report discussing the merits of this curious passive flow control method.

1.2   Literature Review

1.2.1   The Spatial Stokes Layer (SSL)

Description

The Stokes layer is one of the few known exact solutions to the Navier-Stokes equation describing the motion of a viscous fluid as a function of the wall normal coordinate y, whereby the infinitely long wall is located at the bottom at $y = 0$ and oscillating harmonically in its own plane [29]. It turns out that the resulting oscillation in the fluid is only of significant magnitude very close to the wall in a so-called "Stokes layer" and is significantly damped outside of the said-layer.

Jung et al. [8] were the first to suggest using a wall oscillating in the spanwise direction to reduce skin friction in 1992, exploiting the above phenomenon to obtain a maximum drag reduction of 40% at a non-dimensional period of $T^+ = 100$ using direct numerical simulation (DNS), a computational fluid dynamics (CFD) method [30]. The + superscript denotes non-dimensionalisation by wall units, which is based upon the wall friction velocity $u_\tau = \sqrt{\frac{\tau_w}{\rho}}$, along with the kinematic viscosity $\nu = \frac{\mu}{\rho}$, where τ_w is the wall shear stress of the fluid flow, ρ is the density of the fluid, and μ is the dynamic viscosity of the fluid flow. The spanwise velocity of the wall is given by

$$W_w = A \sin\left(\frac{2\pi}{T} t\right),\tag{1.1}$$

where A and T denotes the oscillation amplitude and period, and t denotes time. Moreover, when only one of the channel walls were oscillating, "the reduction in turbulence activity was observed

only near the oscillating wall, while the flow at the other wall remained fully turbulent" [8]. When phase averaged this coincides with the Stokes layer with temporal forcing [10], we will therefore name it temporal Stokes layer (TSL). Dhanak and Si [31] observed that the duration of sweep events were reduced by 47% and their strength reduced by 23%, suggesting that the skin-friction reduction is a result of the "attenuation in the formation of streamwise streaks [30].

As this is a form of active flow control, despite significant drag reductions, significant energy must also be expended to overcome the extra shear stress to create the spanwise motion of the fluid [10]. Baron and Quadrio [32] was the first to consider the net energy savings from spanwise wall oscillation, and it is now accepted that the net energy savings is 10% [10, 30]. However, this technique requires moving parts and therefore requires actuators, which is hard to implement in practical applications especially in transport applications.

Viotti et al. [10] sought to extend the TSL from a time-dependent forcing to a stationary, spatial forcing, which potentially allows an extension into passive solutions which can emulate the oscillation varying over space instead of time (such as the WW). (———————————————————————————————————— kim and hussain———————————————???) Letting x be the streamwise coordinate, y the wall-normal coordinate, and z the spanwise coordinate, the spatial forcing law can be seen in Figure 1.2, and is given by

$$W_w = A \sin\left(\frac{2\pi}{\lambda_x} x\right), \tag{1.2}$$

where A and λ_x denotes the forcing amplitude and the forcing wavelength in the x direction respectively. We will call this flow the spatial Stokes layer (SSL).

Figure 1.2: Schematic of spanwise wall forcing from [10].
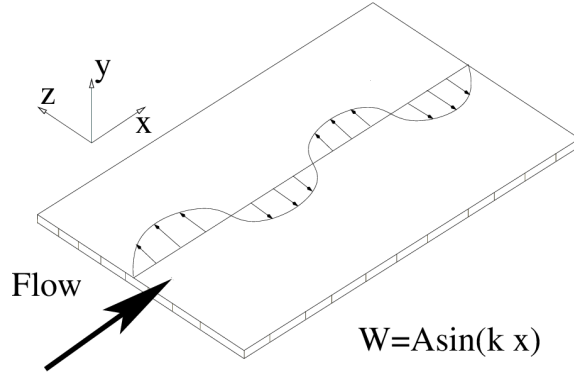
Solving for Velocity

We will now analyse SSL flow analytically following Chernyshenko [28], who ultimately derives their analysis from Viotti et al. [10]. We begin by solving for the velocity profile of SSL flow by first defining the triple decomposition of velocity as follows

$$\mathbf{U} = \overline{\mathbf{U}} + \tilde{\mathbf{u}} + \mathbf{u}', \tag{1.3}$$

where $\overline{\mathbf{U}}$ is the velocity averaged over time, and space in the x and z direction, $\tilde{\mathbf{u}}$ is the phase averaged velocity, and $\mathbf{u}'$ is the remaining stochastic turbulent part of the velocity. Unlike the traditional Reynolds decomposition, we have an extra phase dependent term, which is useful for periodic flows such as SSL flow. We can adapt the definition given in [33] to our case and define for some phase angle $\phi_0 = \phi(x_0 + m\lambda_x, z_0 + n\lambda_z)$,

$$\tilde{\mathbf{u}}(y, \phi_0) \equiv \lim_{M \to \infty} \lim_{N \to \infty} \frac{1}{M} \frac{1}{N} \sum_{m=1}^{M} \sum_{n=1}^{N} \mathbf{U}(x_0 + n\lambda_x, y, z_0 + m\lambda_z) - \overline{\mathbf{U}}(y). \tag{1.4}$$

By including this average, we recognise that there will be periodicity in the x component of the flow velocity; we also include periodicity in the z component of the flow velocity since it will be useful for the WW flow, and doesn't affect the definition for the SSL flow, whose phase average has no z dependence and therefore $\tilde{w} = 0$.

Similarly, we can decompose the pressure field as we did velocity into its triple decomposition with $p = \overline{p} + \tilde{p} + p'$, where $\overline{p}$ is the mean pressure (averaged in time, $x - z$ space, and phase), $\tilde{p}$ is the periodically fluctuating phase averaged pressure, and p' is the randomly fluctuating pressure.

With that definition, we can now solve for the phase averaged velocity of the SSL flow. By linearising the BL equations in the wall units of the flow around a linear profile, we ignore the stochastic fluctuations $\mathbf{u}'$ and p', and let $\overline{\mathbf{U}}^+ = (y^+, 0, 0)$. Moreover, SSL is time invariant. Thus, by analysing the order of various values as in [29], and taking $Re \to \infty$, we get

$$y^+ \frac{\partial \tilde{u}^+}{\partial x^+} + \tilde{v}^+ = -\frac{\partial p^+}{\partial x^+} + \frac{\partial^2 \tilde{u}^+}{\partial (y^+)^2} \tag{1.5}$$

$$0 = -\frac{\partial p^+}{\partial y^+} \tag{1.6}$$

$$y^+ \frac{\partial \tilde{w}^+}{\partial x^+} = -\frac{\partial p^+}{\partial z^+} + \frac{\partial^2 \tilde{w}^+}{\partial (y^+)^2} \tag{1.7}$$

$$0 = \frac{\partial \tilde{u}^+}{\partial x^+} + \frac{\partial \tilde{v}^+}{\partial y^+} + \frac{\partial \tilde{w}^+}{\partial z^+}. \tag{1.8}$$

These are the general BL equations (also known as *Prandtl BL equations*) when linearised around a linear mean profile (i.e. where we let $\overline{U}^+ = (y^+, 0, 0)$).

(————————————————————Comparison between laminar and turbulent mean fields: Fig 3 Viotti————————————————)

At the wall ($y^{+s} = 0$), we have $\tilde{u}_s^{+s} = \tilde{v}_s^{+s} = 0$, and $\tilde{w}_s^{+s} = \hat{W}^{+s} e^{ik_x^{+s} x^{+s}}$, where $\hat{W}_s^{+s} = A^{+s}$ is the wall oscillation amplitude, $k_x^{+s} = \frac{2\pi}{\lambda_x^{+s}}$ is the non-dimensional wavenumber, i is the imaginary unit, the subscript s denotes that the variable is related to SSL flow, and the superscript +s denotes non-dimensionalisation by the friction velocity specific to the SSL flow $u_{\tau,s} = \sqrt{\frac{\tau_{w,s}}{\rho}}$, where $\tau_{w,s}$ is the time, space, and phase averaged wall shear stress of the SSL flow. Although strictly speaking this $\tilde{w}_s^{+s}$ at the wall is only the real part of the exponential function (as well as any other phase averaged terms that we prescribe the exponential function for the rest of this report), however analysis is much more easily done using the exponential function and only taking the real part thereof at the very end. Moreover, since the wall is flat, we expect the pressure gradient in all directions to be zero. We also only expect the spanwise periodic fluctuations to be non-zero,

therefore $\tilde{u}_{\rm s} = \tilde{v}_{\rm s} = 0$. This means that to solve for $\tilde{w}^{+{\rm s}}$ we only need Equation (1.7).

Finally, we expect the spanwise velocity to vary not only in x (due to the x dependence of the prescribed spanwise wall forcing), but also in y as the Stokes layer decreases in strength away from the wall. Therefore, we get

$$\tilde{w}^{+{\rm s}}\left(x^{+{\rm s}}, \check{y}^{+{\rm s}}\right) = \hat{W}_{\rm s}^{+{\rm s}} \check{w}_{\rm s}^{+{\rm s}} e^{i k_x^{+{\rm s}} x^{+{\rm s}}}, \tag{1.9}$$

where we define $y^+ = (k_x^+)^{-1/3} \check{y}^+$ in order to simplify or equations later, and $\check{w}_{\rm s}^{+{\rm s}} = \check{w}_{\rm s}^{+{\rm s}}(\check{y}^{+{\rm s}})$ as the only part of $\tilde{w}^{+{\rm s}}$ dependent on $\check{y}^{+{\rm s}}$. Therefore Equation (1.7) becomes

$$\left(k_x^{+{\rm s}}\right)^{-1/3} \check{y}^{+{\rm s}} \frac{\partial}{\partial x^{+{\rm s}}} \left(\hat{W}^{+{\rm s}} \check{w}_{\rm s}^{+{\rm s}} e^{i k_x^{+{\rm s}} x^{+{\rm s}}}\right) = \frac{\partial^2}{\partial \left((k_x^{+{\rm s}})^{-1/3} \check{y}\right)^2} \left(\hat{W}^{+{\rm s}} \check{w}_{\rm s}^{+{\rm s}} e^{i k_x^{+{\rm s}} x^{+{\rm s}}}\right)$$

$$i \check{y}^{+{\rm s}} \check{w}_{\rm s}^{+{\rm s}} = \frac{{\rm d}^2 \check{w}_{\rm s}^{+{\rm s}}}{{\rm d}(\check{y}^{+{\rm s}})^2}. \tag{1.10}$$

We can see that we can solve for $\check{w}_{\rm s}^{+{\rm s}}$ with only an ordinary differential equation (ODE). We know that at $\check{y}^{+{\rm s}} = 0$, $\check{w}_{\rm s}^{+{\rm s}} = 1$, and since this is a Stokes layer, we want $\check{w}_{\rm s}^{+{\rm s}} \to 0$ as $\check{y}^{+{\rm s}} \to \infty$. This ODE can either be solved numerically or be described by an Airy function (denoted ${\rm Ai}(\cdot)$) as follows,

$$\check{w}_{\rm s}^{+{\rm s}}(\check{y}^{+{\rm s}}) = \frac{{\rm Ai}\left(-i \check{y}^{+{\rm s}} e^{-\frac{4}{3} i \pi}\right)}{{\rm Ai}(0)}, \tag{1.11}$$

which gives

$$w_{\rm s}^{+{\rm s}} = {\rm Re}\left[\hat{W}_{\rm s}^{+{\rm s}} e^{i k_x^{+{\rm s}} x} \frac{{\rm Ai}\left(-i \check{y}^{+{\rm s}} e^{-\frac{4}{3} i \pi}\right)}{{\rm Ai}(0)}\right]. \tag{1.12}$$

Net Power Definition

Our ultimate goal is of course to find how much energy we might be able to save using SSL. We will calculate the net power saved by having SSL in both the top and bottom wall of an infinite flat channel (which was what was done in Viotti et al. [10] such that comparisons can be made with DNS, which requires a finite domain), compared with a reference channel flow with no movement. We will denote variables relating to the reference flow with a subscript 0, and similar to the SSL flow, we will denote non-dimensionalisation by the wall units of the reference flow with the superscript $+0$.

To find this elusive net power saving, we start with conservation of energy in the channel. Thus,

$$P_{\rm in}^+ = P_{\rm out}^+, \tag{1.13}$$

where P denotes power per unit area. We know for SSL, $P_{\rm in}$ includes some sort of external pump that powers the flow against drag (which we hope is reduced from the reference flow), as well as an actuator or motor which drives the oscillatory in-plane wall motion. Whereas for the reference flow $P_{\rm in}$ does not have the latter. On the other hand, the $P_{\rm out}$ of the system is purely through losses in heat, which comes from dissipation in the fluid, which, per unit area, is given by

$$\Phi^+ = \int_0^\infty \overline{\left(\frac{{\rm d}\mathbf{U}^+}{{\rm d}y^+}\right)^2} \, {\rm d}y^+, \tag{1.14}$$

for one wall, where the overbar denotes conducting averaging and phase averaging in time and space in the x, z directions. Despite this being channel flow, we integrate to infinity instead of the channel half height as the analysis is easier to deal with and it is presumed that $\frac{\mathrm{d}\mathbf{U}^+}{\mathrm{d}y^+} \to 0$ quickly as $y^+ \to \infty$ outside the boundary layer. Using the incredibly useful triple decomposition, the dissipation per unit area becomes

$$\Phi^+ = \int_0^\infty \overline{\left(\frac{\mathrm{d}}{\mathrm{d}y^+}\left(\overline{\mathbf{U}}^+ + \tilde{\mathbf{u}}^+ + \mathbf{u}'\right)\right)^2} \, \mathrm{d}y^+ \tag{1.15}$$

$$= \int_0^\infty \left[\overline{\left(\frac{\mathrm{d}\overline{\mathbf{U}}}{\mathrm{d}y^+}\right)^2} + \overline{\left(\frac{\mathrm{d}\tilde{\mathbf{u}}}{\mathrm{d}y^+}\right)^2} + \overline{\left(\frac{\mathrm{d}\mathbf{u}'}{\mathrm{d}y^+}\right)^2} + 2\overline{\left(\frac{\mathrm{d}\overline{\mathbf{U}}}{\mathrm{d}y^+}\frac{\mathrm{d}\tilde{\mathbf{u}}}{\mathrm{d}y^+} + \frac{\mathrm{d}\overline{\mathbf{U}}}{\mathrm{d}y^+}\frac{\mathrm{d}\mathbf{u}'}{\mathrm{d}y^+} + \frac{\mathrm{d}\tilde{\mathbf{u}}}{\mathrm{d}y^+}\frac{\mathrm{d}\mathbf{u}'}{\mathrm{d}y^+}\right)}^{\nearrow 0} \right] \mathrm{d}y^+ \tag{1.16}$$

$$= \int_0^\infty \overline{\left(\frac{\mathrm{d}\overline{\mathbf{U}}}{\mathrm{d}y^+}\right)^2} \, \mathrm{d}y^+ + \int_0^\infty \overline{\left(\frac{\mathrm{d}\tilde{\mathbf{u}}}{\mathrm{d}y^+}\right)^2} \, \mathrm{d}y^+ + \int_0^\infty \overline{\left(\frac{\mathrm{d}\mathbf{u}'}{\mathrm{d}y^+}\right)^2} \, \mathrm{d}y^+ \, . \tag{1.17}$$

Wonderfully, the cross terms inside the final brackets of 1.16 all go to zero since the over-bar for dissipation involves both the mean averaging and phase averaging, and since $\overline{\overline{a}b} = \overline{a}\overline{b}$ for any a, b, and the average of a fluctuating quantity is zero. Moreover, the flows being considered throughout the rest of the report do not have a mean velocity in the y or z direction, and $\frac{\mathrm{d}\tilde{v}}{\mathrm{d}y^+} \approx 0$ compared to the other dissipation rates in the BL. We can therefore reduce the dissipation further to

$$\Phi^+ = \int_0^\infty \overline{\left(\frac{\mathrm{d}\overline{U}}{\mathrm{d}y^+}\right)^2} \, \mathrm{d}y^+ + \int_0^\infty \overline{\left(\frac{\mathrm{d}}{\mathrm{d}y^+}(\tilde{u}, \tilde{v}, \tilde{w})\right)^2} \, \mathrm{d}y^+ + \int_0^\infty \overline{\left(\frac{\mathrm{d}\mathbf{u}'}{\mathrm{d}y^+}\right)^2} \, \mathrm{d}y^+ \tag{1.18}$$

$$= \int_0^\infty \overline{\left(\frac{\mathrm{d}\overline{U}}{\mathrm{d}y^+}\right)^2} \, \mathrm{d}y^+ + \int_0^\infty \overline{\left(\frac{\mathrm{d}\tilde{u}}{\mathrm{d}y^+}\right)^2} \, \mathrm{d}y^+ + \int_0^\infty \overline{\left(\frac{\mathrm{d}\tilde{w}}{\mathrm{d}y^+}\right)^2} \, \mathrm{d}y^+ + \int_0^\infty \overline{\left(\frac{\mathrm{d}\mathbf{u}'}{\mathrm{d}y^+}\right)^2} \, \mathrm{d}y^+ \tag{1.19}$$

$$\equiv \Phi_{\overline{U}}^+ + \Phi_{\tilde{u}}^+ + \Phi_{\tilde{w}}^+ + \Phi_{\mathbf{u}'}^+. \tag{1.20}$$

For the reference flow $\Phi_0^{+0} = \Phi_{\overline{U},0}^{+0} + \Phi_{\mathbf{u}',0}^{+0}$, whereas for the SSL flow $\Phi_s^{+s} = \Phi_{\overline{U},s}^{+s} + \Phi_{\tilde{w},s}^{+s} + \Phi_{\mathbf{u}',s}^{+s}$. Therefore we can call the $\overline{U}$ and $\mathbf{u}'$ portions of dissipation drag, and the extra $\tilde{w}$ portion of dissipation an extra required portion for the SSL flow.

Let us now define the net power reduction of the SSL channel flow as a percentage of the reference channel flow as follows,

$$P_{\text{net,s}} \equiv 100\% \frac{2\Phi_0^{+0} - 2\Phi_s^{+0}}{2\Phi_0^{+0}} \tag{1.21}$$

$$= 100\% \frac{\Phi_{\overline{U},0}^{+0} + \Phi_{\mathbf{u}',0}^{+0} - \left(\Phi_{\overline{U},s}^{+0} + \Phi_{\tilde{w},s}^{+0} + \Phi_{\mathbf{u}',s}^{+0}\right)}{\Phi_0^{+0}} \tag{1.22}$$

$$= 100\% \frac{\left(\Phi_{\overline{U},0}^{+0} - \Phi_{\overline{U},s}^{+0}\right) + \left(\Phi_{\mathbf{u}',0}^{+0} - \Phi_{\mathbf{u}',s}^{+0}\right)}{\Phi_0^{+0}} + 100\% \frac{\left(0 - \Phi_{\tilde{w},s}^{+0}\right)}{\Phi_0^{+0}} \tag{1.23}$$

$$= 100\% \frac{\Delta\Phi_{\overline{U},s}^{+0} + \Delta\Phi_{\mathbf{u}',s}^{+0}}{\Phi_0^{+0}} + 100\% \frac{\Delta\Phi_{\tilde{w},s}^{+0}}{\Phi_0^{+0}} \tag{1.24}$$

$$\equiv P_{\text{sav,s}} + P_{\text{req,s}}, \tag{1.25}$$

where $P_{\text{sav,s}}$ and $P_{\text{req,s}}$ are the resulting power saved due to drag reduction and power required to maintain forcing to counteract spanwise velocity gradients respectively; both are expressed as

a percentage of the power required to drive the reference flow. The definition here is numerically equivalent to that of Viotti et al. [10], which defines them as a function of dimensional units.

Power Saved from SSL Wall Forcing

$P_{\mathrm{sav,s}}$ was obtained from DNS results from Viotti et al. [10], which was again conducted at $Re_\tau = 200$ using different forcing wavelengths λ_x^{+0}, and forcing amplitudes $\hat{W}_{\mathrm{s}}^{+0} = 1, 2, 6, 12$. Chernyshenko [28] only used data up to $\lambda_x^{+0} < 3000$, which was digitised via the web app *WebPlot-Digitizer*, and fitted $P_{\mathrm{sav,s}}$ at each $\hat{W}_{\mathrm{s}}^{+0}$ on a degree 5 polynomial of λ_x^{+0}, i.e.

$$P_{\mathrm{sav,s}} = f\left(\lambda_x^{+0}, \hat{W}_{\mathrm{s}}^{+0}\right) \tag{1.26}$$

$$= c_{0,\hat{W}_{\mathrm{s}}^{+0}} + c_{1,\hat{W}_{\mathrm{s}}^{+0}}\lambda_x^{+0} + c_{2,\hat{W}_{\mathrm{s}}^{+0}}\left(\lambda_x^{+0}\right)^2 + c_{3,\hat{W}_{\mathrm{s}}^{+0}}\left(\lambda_x^{+0}\right)^3 + c_{4,\hat{W}_{\mathrm{s}}^{+0}}\left(\lambda_x^{+0}\right)^4 + c_{5,\hat{W}_{\mathrm{s}}^{+0}}\left(\lambda_x^{+0}\right)^5, \tag{1.27}$$

where the coefficients are given in Table 1.1. The data and curve fits thereof are shown in Figure 1.3

$\hat{W}_{\mathrm{s}}^{+0}$	c_0	c_1	c_2	c_3	c_4	c_5
1	1.135	0.002929	-1.205×10^{-6}	1.447×10^{-10}	-1.047×10^{-13}	2.609×10^{-17}
2	-1.856	0.03954	-5.285×10^{-5}	3.498×10^{-8}	-1.127×10^{-11}	1.328×10^{-15}
6	15.25	0.04888	-4.441×10^{-5}	1.628×10^{-8}	-2.845×10^{-12}	1.938×10^{-16}
12	27.90	0.03824	-2.810×10^{-5}	8.015×10^{-9}	-1.082×10^{-12}	5.535×10^{-17}

Table 1.1: Coefficients of curve fits of $P_{\mathrm{sav,s}}$ data from DNS for different forcing wavelength λ_x^{+0} using different forcing amplitudes $\hat{W}_{\mathrm{s}}^{+0}$ by Viotti et al. [10]

Power Required to Drive SSL Wall Forcing

In order to find $P_{\mathrm{req,s}}$, we begin by expressing $\Delta\Phi_{\tilde{w},\mathrm{s}}^{+0} = -\Phi_{\tilde{w},\mathrm{s}}^{+0}$ in the wall units of the SSL flow. This requires recognising that dissipation per unit area Φ has the units of power per unit area, which is equivalent to velocity times force per unit area. This means that Φ^+ is non-dimensionalised with the relevant $u_\tau \tau_w$. We will use that below to get

$$\Phi_{\tilde{w},\mathrm{s}}^{+0} = \frac{\Phi_{\tilde{w},\mathrm{s}}}{u_{\tau,0}\tau_{w,0}} \tag{1.28}$$

$$= \frac{\Phi_{\tilde{w},\mathrm{s}}}{u_{\tau,\mathrm{s}}\tau_{w,\mathrm{s}}} \frac{u_{\tau,\mathrm{s}}\tau_{w,\mathrm{s}}}{u_{\tau,0}\tau_{w,0}} \tag{1.29}$$

$$= \Phi_{\tilde{w},\mathrm{s}}^{+\mathrm{s}} \left(\frac{\tau_{w,\mathrm{s}}}{\tau_{w,0}}\right)^{3/2}. \tag{1.30}$$
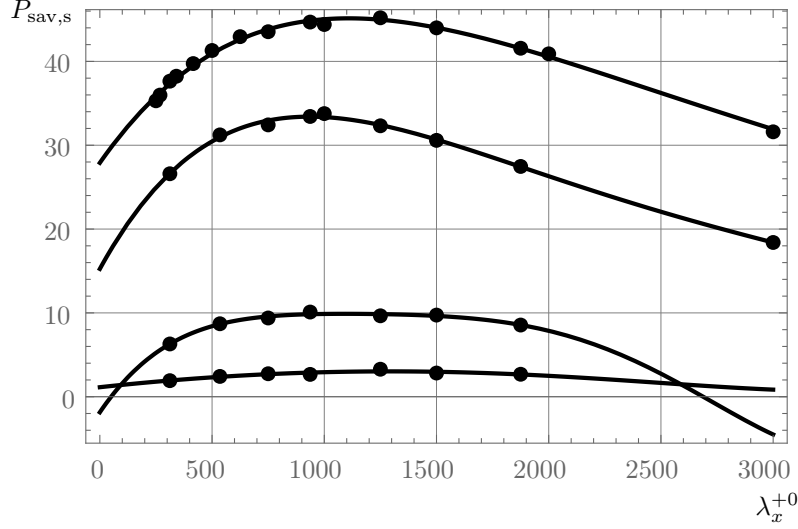
Figure 1.3: Power saved due to drag reduction in the SSL flow, $P_{\text{sav,s}}$, as a function of wall forcing wavelength λ_x^{+0}. The curve fits from Chernyshenko [28] and corresponding data from Viotti et al. [10] are for forcing amplitudes $\hat{W}_{\text{s}}^{+0} = 1, 2, 6, 12$ which are in order from the bottom to top curve. The figure is slightly modified from [28].

Now we will find $\Phi_{\tilde{w},\text{s}}^{+\text{s}}$ by using Equation (1.9) as follows

$$\Phi_{\tilde{w},\text{s}}^{+\text{s}} = \int_0^\infty \overline{\left(\frac{\mathrm{d}\tilde{w}_{\text{s}}^{+\text{s}}}{\mathrm{d}y^{+\text{s}}}\right)^2} \, \mathrm{d}y^{+\text{s}} \tag{1.31}$$

$$= \int_0^\infty \left(\frac{\mathrm{d}\overline{\hat{W}_{\text{s}}^{+\text{s}}\check{w}_{\text{s}}^{+\text{s}}e^{ik_x^{+\text{s}}x^{+\text{s}}}}}{\mathrm{d}\left((k_x^{+\text{s}})^{-1/3}\check{y}^{+\text{s}}\right)}\right)^2 \mathrm{d}\left((k_x^{+\text{s}})^{-1/3}\check{y}^{+\text{s}}\right) \tag{1.32}$$

$$= \left(\hat{W}_{\text{s}}^{+\text{s}}\right)^2 \left(k_x^{+\text{s}}\right)^{1/3} \int_0^\infty \frac{1}{2}\left|\frac{\mathrm{d}\check{w}_{\text{s}}^{+\text{s}}}{\mathrm{d}\check{y}^{+\text{s}}}\right|^2 \mathrm{d}\check{y}^{+\text{s}}. \tag{1.33}$$

Since $\check{w}_{\text{s}}^{+\text{s}}$ is a known function that we found in Equation (1.11), it is possible to evaluate the integral numerically. Chernyshenko [28] gives $\int_0^\infty \frac{1}{2}\left(\frac{\mathrm{d}\check{w}_{\text{s}}^{+\text{s}}}{\mathrm{d}\check{y}^{+\text{s}}}\right)^2 \mathrm{d}\check{y}^{+\text{s}} = 0.3157$. For the other two terms, we wish to non-dimensionalise them with $^{+0}$units similar to Equation (1.30), as that is the units that are presented in Viotti et al. [10], whose data we will use for calculating both $P_{\text{net,s}}$ and $P_{\text{net,w}}$. Thus,

$$k_x^{+\text{s}} = \frac{2\pi}{\lambda_x^{+\text{s}}} = \frac{2\pi}{\lambda u_{\tau,\text{s}}/\nu}\frac{u_{\tau,0}/\nu}{u_{\tau,0}/\nu} = \frac{2\pi}{\lambda_x^{+0}}\left(\frac{\tau_{w,\text{s}}}{\tau_{w,0}}\right)^{-1/2}, \tag{1.34}$$

and

$$\hat{W}_{\text{s}}^{+\text{s}} = \frac{\hat{W}_{\text{s}}}{u_{\tau,\text{s}}}\frac{u_{\tau,0}}{u_{\tau,0}} = \hat{W}_{\text{s}}^{+0}\left(\frac{\tau_{w,\text{s}}}{\tau_{w,0}}\right)^{-1/2}. \tag{1.35}$$

The ratio of wall shear stress is incredibly useful, as by the definition of $P_{\text{sav,s}}$, it is equivalent to

$$P_{\text{sav,s}} = 100\%\frac{\tau_{w,0} - \tau_{w,\text{s}}}{\tau_{w,0}} \implies \frac{\tau_{w,\text{s}}}{\tau_{w,0}} = 1 - \frac{P_{\text{sav,s}}}{100\%}. \tag{1.36}$$

Finally, we know that for the flat plate reference flow the dissipation on one side of the channel is given by $\Phi_0^{+0} = U_b^{+0}$, where U_b is the bulk velocity (the time and space averaged velocity in the channel) [28]. Definitionally, the coefficient of friction of a flow based on the bulk velocity is given

15

by $C_f = \frac{\tau_w}{\frac{1}{2}\rho U_b} = \frac{2u_\tau}{U_b} = \frac{2}{U_b^+}$. Therefore,

$$\Phi_0^{+0} = U_b^{+0} = \sqrt{\frac{2}{C_{f,0}}}. \tag{1.37}$$

DNS by Viotti et al. [10] at $Re_\tau = 200$ was in good correlation with the estimate $C_{f,0} = 0.0336Re_\tau^{-0.273}$ given by [34], where Re_τ is the friction Reynolds number, defined using the friction velocity u_τ and channel half height h as the characteristic velocity and length respectively. As in [10, 28], we will use this estimate. Thus, from the definition of $P_{\text{req,s}}$ in Equation (1.25), and by using Equations (1.30), (1.33), (1.34), (1.35), (1.36), and (1.37), we get

$$P_{\text{req,s}} = -100\%\frac{\Phi_s^{+0}}{\Phi_0^{+0}} \tag{1.38}$$

$$= -100\% \left(\hat{W}_s^{+0}\right)^2 \sqrt{\frac{C_{f,0}}{2}} \left(\frac{2\pi}{\lambda_x^{+s}}\left(1 - \frac{P_{\text{sav,s}}}{100\%}\right)\right)^{1/3} \int_0^\infty \frac{1}{2}\left|\frac{\mathrm{d}\breve{w}_s^{+s}}{\mathrm{d}\breve{y}^{+s}}\right|^2 \mathrm{d}\breve{y}^{+s} \tag{1.39}$$

$$= -100\%(0.3157)\left(\hat{W}_s^{+0}\right)^2 \sqrt{\frac{C_{f,0}}{2}} \left(\frac{2\pi}{\lambda_x^{+s}}\left(1 - \frac{P_{\text{sav,s}}}{100\%}\right)\right)^{1/3}. \tag{1.40}$$

By inserting $P_{\text{sav,s}}$ from Equation (1.27) for each $\hat{W}_s^{+0}$ with the corresponding coefficients from Table 1.1, we will find $P_{\text{req,s}}$. We plot in Figure 1.4
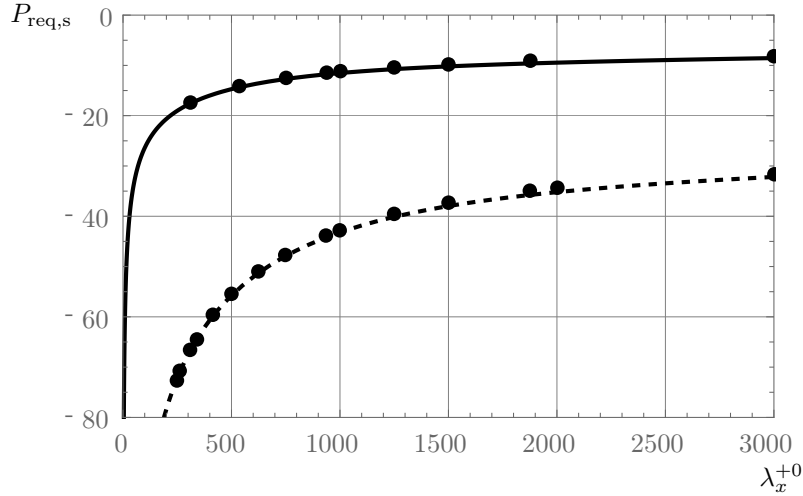
Figure 1.4: Power required to drive the forcing in the SSL flow, $P_{\text{req,s}}$, as a function of wall forcing wavelength λ_x^{+0} from Equation (1.40) at $\hat{W}_s^{+0} = 6$ (solid) and $\hat{W}_s^{+0} = 12$ (dashed) with corresponding DNS data from Viotti et al. [10]. The figure is slightly modified from [28].

SSL Final Results

By using Equation (1.25), which says $P_{\text{net,s}} = P_{\text{sav,s}} + P_{\text{req,s}}$, the results for $\hat{W}_s^{+0}$ along with its corresponding DNS data are plotted in Figure 1.5. Based on these results of Viotti et al. [10] at their parameters, it can be shown that a maximum net power decrease of 23% at $\hat{W}_s^{+0} = 6$ and at $\lambda_x^{+0} = 1000 - 1250$.

Other results presented by Viotti et al. [10], include the clear modification of the near-wall turbulence compared to the reference case, with much fewer turbulent vortical structures visible

based on a λ_2^{+0} quantity introduced by Jeong and Hussain [35] that they set at -0.03 that we will not discuss here. They also found a reduction of the turbulence intensity (the root-mean-square of turbulent fluctuations). Most importantly for this project, they found that, like other DR techniques (such as riblets), "[t]he DR manifests itself through the thickening of the viscous sublayer, which results in the upward shift of the logarithmic portion of the velocity profile" [10]. This result will be explored later in this report. (————————————————-section?————————————————————-)
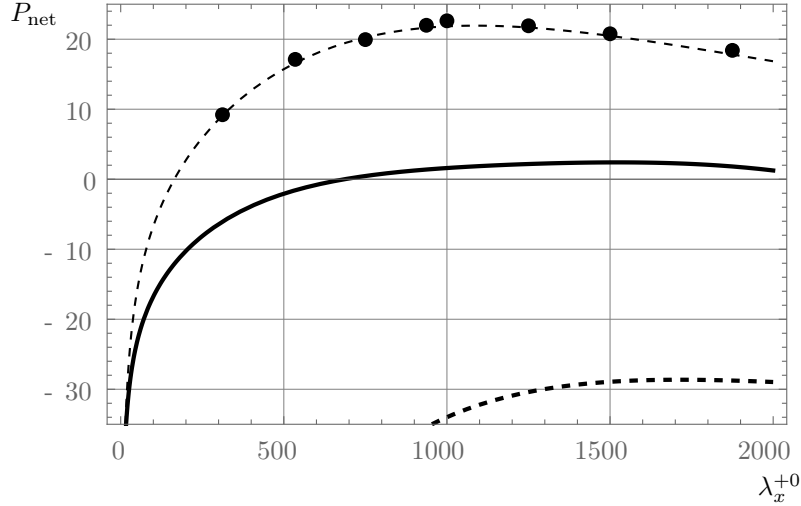
Figure 1.5: Net power reduction P_{net} as a function of wall forcing wavelength λ_x^{+0} for SSL at $\hat{W}_s^{+0} = 6$ (thin-dashes) corresponding DNS data from Viotti et al. [10], and for WW at prescribed $\hat{W}_s^{+0} = 2$ (solid) and at $\hat{W}_s^{+0} = 6$ (thick-dashes). The figure is slightly modified from [28].

1.2.2 Analysis of The Oblique Wavy Wall (WW)

Description

As mentioned in Section 1.1, TSL and SSL are active control strategy, which requires actuators. Several mechanisms are being trialed in laboratories experimentally to effect TSL or SSL such as dielectric-barrier discharge plasma actuators [36], azimuthally moving pipe walls [37], etc. However, as these actuators have low TRL, SSL was conjectured, analysed, and simulated via CFD mainly so that a passive device (most likely via wall roughness) could emulate the flow patterns to affect the TBL the same way to reduce drag. In fact, Viotti et al. [10] mentions a patent for riblets that would oscillate sinusoidally in the streamwise direction [38]; the idea has been briefly studied although the positive effects of small amplitudes "could not be determined outside the uncertainty range", whilst the larger amplitudes actually reduce the total drag reduction due to increase in pressure drag [39]. The same authors claimed that a 1.3% drag reduction was possible [40] More research should be done on that to better evaluate its viability.

In [28], Chernyshenko proposes instead to use an undulating wavy wall (WW) placed at an oblique angle to the direction of the flow (Figure 1.6). Since this wavy wall is at an angle

to the streamwise direction, it creates a spanwise pressure gradient that accelerates it towards the crests when approaching them and when leaving them. This oscillatory force that the fluid experiences generates alternating spanwise motion [41]. A visualisation of the SSL forcing and WW in Figure 1.7 shows the similarities (and differences) in the spanwise oscillation. We will now follow Chernyshenko [28] in their calculation of the net power reduction of WW, $P_{\mathrm{net,w}}$.
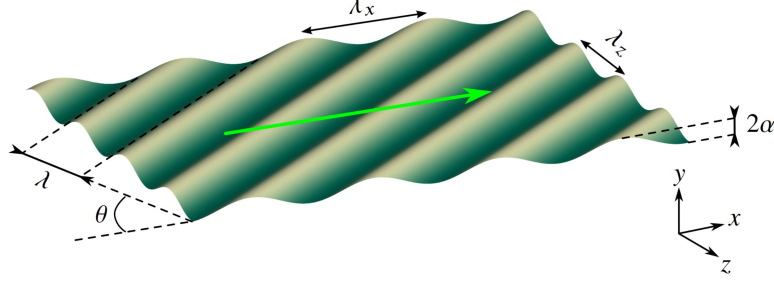
Figure 1.6: Schematic of the oblique wavy wall from [42]. The green arrow represents the flow direction, at an oblique angle θ to the wavy wall.
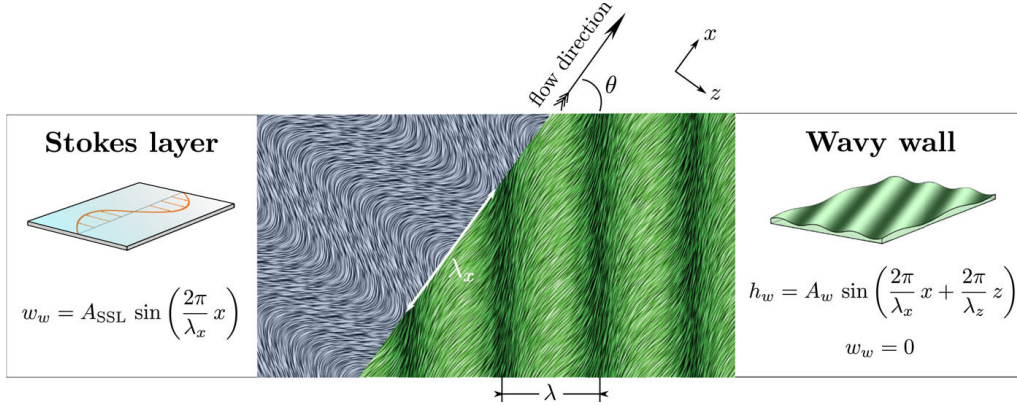
Figure 1.7: An emulation of the forcing by SSL (left) and WW (right) showing mean streaklines close to the wall, where the background is coloured according to the norm of the velocity vector. Figure from [41]. Here $A_w = \alpha$ from Figure 1.6

Phase Averaged Velocity

To find the net power reduction we again start with the BL equations linearised around a linear profile, Equations (1.5)–(1.8). However, since there are undulations along the wall, we will let the y coordinate follow the contours of the wall. Hence by the no-slip and inpenetrability conditions, we have that at the wall $U_{\mathrm{w}}^{+\mathrm{w}} = V_{\mathrm{w}}^{+\mathrm{w}} = W_{\mathrm{w}}^{+\mathrm{w}} = 0$, and accordingly $\tilde{u}_{\mathrm{w}}^{+\mathrm{w}} = \tilde{v}_{\mathrm{w}}^{+\mathrm{w}} = \tilde{w}_{\mathrm{w}}^{+\mathrm{w}} = 0$ at the wall. Unlike the SSL case, we now have variations in pressure. This pressure variation is "proportional to the velocity at the outer edge of the boundary layer and to the displacement magnitude" and occurs as a result of the displacement of streamlines caused by variations in the shape of the wall surface, which "is passed with little change to the streamlines at the outer edge of the boundary layer, where the flow velocity is large" [28]. (————

—————————————————————————————————This can be shown with the bernoulli

equation ——————————————————————————-) This means that the phase averaged pressure does not vary in the wall normal direction and can then be assumed to have the form $\tilde{p}_{\mathrm{w}}^{+\mathrm{w}} = \hat{P}_{\mathrm{w}}^{+\mathrm{w}} e^{i\left(k_x^{+\mathrm{w}} x^{+\mathrm{w}} + k_z^{+\mathrm{w}} z^{+\mathrm{w}}\right)}$. The phase averaged velocity is a function of x, y, z and is then $\left(\tilde{u}_{\mathrm{w}}^{+\mathrm{w}}, \tilde{v}_{\mathrm{w}}^{+\mathrm{w}}, \tilde{w}_{\mathrm{w}}^{+\mathrm{w}}\right) = \left(\hat{U}_{\mathrm{w}}^{+\mathrm{w}}(y), \hat{V}_{\mathrm{w}}^{+\mathrm{w}}(y), \hat{W}_{\mathrm{w}}^{+\mathrm{w}}(y)\right) e^{i\left(k_x^{+\mathrm{w}} x^{+\mathrm{w}} + k_z^{+\mathrm{w}} z^{+\mathrm{w}}\right)}$. By substituting the above into the BL equations without the unnecessary y-momentum equation, (i.e. Equations (1.5), (1.7), (1.8)), we get

$$ik_x^{+\mathrm{w}} y^{+\mathrm{w}} \hat{U}_{\mathrm{w}}^{+\mathrm{w}} + \hat{V}_{\mathrm{w}}^{+\mathrm{w}} = -ik_x^{+\mathrm{w}} \hat{P}_{\mathrm{w}}^{+\mathrm{w}} + \frac{\mathrm{d}^2 \hat{U}_{\mathrm{w}}^{+\mathrm{w}}}{\mathrm{d}\left(y^{+\mathrm{w}}\right)^2} \tag{1.41}$$

$$ik_x^{+\mathrm{w}} y^{+\mathrm{w}} \hat{W}_{\mathrm{w}}^{+\mathrm{w}} = -ik_z \hat{P}_{\mathrm{w}}^{+\mathrm{w}} + \frac{\mathrm{d}^2 \hat{W}_{\mathrm{w}}^{+\mathrm{w}}}{\mathrm{d}\left(y^{+\mathrm{w}}\right)^2} \tag{1.42}$$

$$ik_x^{+\mathrm{w}} \hat{U}_{\mathrm{w}}^{+\mathrm{w}} + \frac{\mathrm{d}\hat{V}_{\mathrm{w}}^{+\mathrm{w}}}{\mathrm{d}y^{+\mathrm{w}}} + ik_z^{+\mathrm{w}} \hat{W}_{\mathrm{w}}^{+\mathrm{w}} = 0. \tag{1.43}$$

Now we eliminate $\hat{V}_{\mathrm{w}}^{+\mathrm{w}}$ by substituting $\hat{V}_{\mathrm{w}}^{+\mathrm{w}}$ from Equation (1.41) into the second term of Equation (1.43) to get

$$ik_x^{+\mathrm{w}} \hat{U}_{\mathrm{w}}^{+\mathrm{w}} + \frac{\mathrm{d}}{\mathrm{d}y^{+\mathrm{w}}}\left(-ik_x^{+\mathrm{w}} y^{+\mathrm{w}} \hat{U}_{\mathrm{w}}^{+\mathrm{w}} - ik_x^{+\mathrm{w}} \hat{P}_{\mathrm{w}}^{+\mathrm{w}} + \frac{\mathrm{d}^2 \hat{U}_{\mathrm{w}}^{+\mathrm{w}}}{\mathrm{d}\left(y^{+\mathrm{w}}\right)^2}\right) + ik_z^{+\mathrm{w}} \hat{W}_{\mathrm{w}}^{+\mathrm{w}} = 0 \tag{1.44}$$

$$ik_x^{+\mathrm{w}} \hat{U}_{\mathrm{w}}^{+\mathrm{w}} - ik_x^{+\mathrm{w}}\left(\hat{U}_{\mathrm{w}}^{+\mathrm{w}} + y^{+\mathrm{w}} \frac{\mathrm{d}\hat{U}_{\mathrm{w}}^{+\mathrm{w}}}{\mathrm{d}y^{+\mathrm{w}}}\right) + \frac{\mathrm{d}^3 \hat{U}_{\mathrm{w}}^{+\mathrm{w}}}{\mathrm{d}\left(y^{+\mathrm{w}}\right)^3} + ik_z^{+\mathrm{w}} \hat{W}_{\mathrm{w}}^{+\mathrm{w}} = 0 \tag{1.45}$$

$$-ik_x^{+\mathrm{w}} y^{+\mathrm{w}} \frac{\mathrm{d}\hat{U}_{\mathrm{w}}^{+\mathrm{w}}}{\mathrm{d}y^{+\mathrm{w}}} + \frac{\mathrm{d}^3 \hat{U}_{\mathrm{w}}^{+\mathrm{w}}}{\mathrm{d}\left(y^{+\mathrm{w}}\right)^3} + ik_z^{+\mathrm{w}} \hat{W}_{\mathrm{w}}^{+\mathrm{w}} = 0. \tag{1.46}$$

We now let $y^+ = \left(k_x^+\right)^{-1/3} y^+$ which we used in Section 1.2.1 when we solved for the variation of spanwise velocity in y for SSL in order to make this calculation consistent with that of SSL. Furthermore, Chernyshenko [28] calculated that by rescaling as

$$\hat{U}_{\mathrm{w}}^{+\mathrm{w}}\left(y^{+\mathrm{w}}\right) = i\left(k_z^{+\mathrm{w}}\right)^2 \left(k_x^{+\mathrm{w}}\right)^{-5/3} \hat{P}_{\mathrm{w}}^{+\mathrm{w}} \breve{u}_{\mathrm{w}}^{+\mathrm{w}}\left(\breve{y}^{+\mathrm{w}}\right), \tag{1.47}$$

and

$$\hat{W}_{\mathrm{w}}^{+\mathrm{w}}\left(y^{+\mathrm{w}}\right) = ik_z^{+\mathrm{w}}\left(k_x^{+\mathrm{w}}\right)^{-2/3} \hat{P}_{\mathrm{w}}^{+\mathrm{w}} \breve{w}_{\mathrm{w}}^{+\mathrm{w}}\left(\breve{y}^{+\mathrm{w}}\right), \tag{1.48}$$

we can substitute into Equation (1.42) as

$$ik_x^{+\mathrm{w}}\left[\left(k_x^{+\mathrm{w}}\right)^{-1/3} \breve{y}^{+\mathrm{w}}\right]\left[ik_z^{+\mathrm{w}}\left(k_x^{+\mathrm{w}}\right)^{-2/3} \hat{P}_{\mathrm{w}}^{+\mathrm{w}} \breve{w}_{\mathrm{w}}^{+\mathrm{w}}\right] = -ik_z \hat{P}_{\mathrm{w}}^{+\mathrm{w}} + \frac{\mathrm{d}^2\left[ik_z^{+\mathrm{w}}\left(k_x^{+\mathrm{w}}\right)^{-2/3} \hat{P}_{\mathrm{w}}^{+\mathrm{w}} \breve{w}_{\mathrm{w}}^{+\mathrm{w}}\right]}{\mathrm{d}\left(\left(k_x^{+\mathrm{w}}\right)^{-1/3} \breve{y}^{+\mathrm{w}}\right)^2},$$

and Equation (1.46) as

$$ik_x^{+\mathrm{w}}\left[\left(k_x^{+\mathrm{w}}\right)^{-1/3} \breve{y}^{+\mathrm{w}}\right] \frac{\mathrm{d}\left[i\left(k_z^{+\mathrm{w}}\right)^2 \left(k_x^{+\mathrm{w}}\right)^{-5/3} \hat{P}_{\mathrm{w}}^{+\mathrm{w}} \breve{u}_{\mathrm{w}}^{+\mathrm{w}}\right]}{\mathrm{d}\left(\left(k_x^{+\mathrm{w}}\right)^{-1/3} \breve{y}^{+\mathrm{w}}\right)} - ik_z^{+\mathrm{w}}\left[ik_z^{+\mathrm{w}}\left(k_x^{+\mathrm{w}}\right)^{-2/3} \hat{P}_{\mathrm{w}}^{+\mathrm{w}} \breve{w}_{\mathrm{w}}^{+\mathrm{w}}\right]$$

$$= \frac{\mathrm{d}^3\left[i\left(k_z^{+\mathrm{w}}\right)^2 \left(k_x^{+\mathrm{w}}\right)^{-5/3} \hat{P}_{\mathrm{w}}^{+\mathrm{w}} \breve{u}_{\mathrm{w}}^{+\mathrm{w}}\right]}{\mathrm{d}\left(\left(k_x^{+\mathrm{w}}\right)^{-1/3} \breve{y}^{+\mathrm{w}}\right)^3},$$

to get

$$i\breve{y}^{+\mathrm{w}}\breve{w}_{\mathrm{w}}^{+\mathrm{w}} = -1 + \frac{\mathrm{d}^2 \breve{w}_{\mathrm{w}}^{+\mathrm{w}}}{\mathrm{d}\left(\breve{y}^{+\mathrm{w}}\right)^2} \tag{1.49}$$

$$\frac{\mathrm{d}^3 \breve{u}_{\mathrm{w}}^{+\mathrm{w}}}{\mathrm{d}\left(\breve{y}^{+\mathrm{w}}\right)^3} = i\breve{y}^{+\mathrm{w}}\frac{\mathrm{d}\breve{u}_{\mathrm{w}}^{+\mathrm{w}}}{\mathrm{d}\breve{y}^{+\mathrm{w}}} - i\breve{w}_{\mathrm{w}}^{+\mathrm{w}}. \tag{1.50}$$

This system has the boundary conditions $\frac{\mathrm{d}\breve{u}^{+\mathrm{w}}}{\mathrm{d}\breve{y}^{+\mathrm{w}}} \to 0$ and $\breve{w} \to 0$ as $\breve{y}^{+\mathrm{w}} \to \infty$, and $\breve{u}^{+\mathrm{w}} = \breve{w}^{+\mathrm{w}} = 0$ and $\frac{\mathrm{d}^2 \breve{u}_{\mathrm{w}}^{+\mathrm{w}}}{\mathrm{d}(y^{+\mathrm{w}})^2} = \left(\frac{k_x^{+\mathrm{w}}}{k_z^{+\mathrm{w}}}\right)^2$ at $\breve{y}^{+\mathrm{w}} = 0$. The final condition comes from solving Equation (1.41) at $\breve{y}^{+\mathrm{w}} = 0$ (where also $\hat{V}_{\mathrm{w}}^{+\mathrm{w}} = 0$).

Since Equation (1.49) is decoupled from $\breve{u}_{\mathrm{w}}^{+\mathrm{w}}$, we can solve it numerically for $\breve{w}_{\mathrm{w}}^{+\mathrm{w}}$. Then to solve Equation (1.41), we decompose $\breve{u}_{\mathrm{w}}^{+\mathrm{w}}$ into

$$\breve{u}_{\mathrm{w}}^{+\mathrm{w}} = \breve{u}_{w,\mathrm{w}}^{+\mathrm{w}} + \left(\frac{k_x^{+\mathrm{w}}}{k_z^{+\mathrm{w}}}\right)^2 \breve{u}_{p,\mathrm{w}}^{+\mathrm{w}}, \tag{1.51}$$

with $\breve{u}_{w,\mathrm{w}}^{+\mathrm{w}}$ and $\breve{u}_{p,\mathrm{w}}^{+\mathrm{w}}$ satisfying

$$\frac{\mathrm{d}^3 \breve{u}_{w,\mathrm{w}}^{+\mathrm{w}}}{\mathrm{d}\left(\breve{y}^{+\mathrm{w}}\right)^3} = i\breve{y}^{+\mathrm{w}}\frac{\mathrm{d}\breve{u}_{w,\mathrm{w}}^{+\mathrm{w}}}{\mathrm{d}\breve{y}^{+\mathrm{w}}} - i\breve{w}_{\mathrm{w}}^{+\mathrm{w}}, \tag{1.52}$$

where $\frac{\mathrm{d}\breve{u}_{w,\mathrm{w}}^{+\mathrm{w}}}{\mathrm{d}\breve{y}^{+\mathrm{w}}} \to 0$ as $\breve{y}^{+\mathrm{w}} \to \infty$, and $\breve{u}_{w,\mathrm{w}}^{+\mathrm{w}} = \frac{\mathrm{d}^2 \breve{u}_{w,\mathrm{w}}^{+\mathrm{w}}}{\mathrm{d}(\breve{y}^{+\mathrm{w}})^2} = 0$ at $\breve{y}^{+\mathrm{w}} = 0$, and

$$\frac{\mathrm{d}^3 \breve{u}_{p,\mathrm{w}}^{+\mathrm{w}}}{\mathrm{d}\left(\breve{y}^{+\mathrm{w}}\right)^3} = i\breve{y}^{+\mathrm{w}}\frac{\mathrm{d}\breve{u}_{p,\mathrm{w}}^{+\mathrm{w}}}{\mathrm{d}\breve{y}^{+\mathrm{w}}}, \tag{1.53}$$

where $\frac{\mathrm{d}\breve{u}_{p,\mathrm{w}}^{+\mathrm{w}}}{\mathrm{d}\breve{y}^{+\mathrm{w}}} \to 0$ as $\breve{y}^{+\mathrm{w}} \to \infty$, and $\breve{u}_{p,\mathrm{w}}^{+\mathrm{w}} = 0$, $\frac{\mathrm{d}^2 \breve{u}_{p,\mathrm{w}}^{+\mathrm{w}}}{\mathrm{d}(\breve{y}^{+\mathrm{w}})^2} = 1$ at $\breve{y}^{+\mathrm{w}} = 0$. Physically $\breve{u}_{w,\mathrm{w}}^{+\mathrm{w}}$ "corresponds to the perturbation of $[u_{\mathrm{w}}^{+\mathrm{s}}]$ due to wall-normal velocity induced by spanwise velocity dependence on z" whereas $\breve{u}_{p,\mathrm{w}}^{+\mathrm{w}}$ "is related to the perturbation of $[u_{\mathrm{w}}^{+\mathrm{s}}]$ due to the longitudinal pressure gradient induced by the wall" [28]. These ordinary differential equations were then solved numerically by Chernyshenko [28] using Mathematica.

Matching Spanwise Shear Profile with SSL

In order to use the results of Viotti et al. [10], Chernyshenko [28] had the idea to matching the spanwise profiles between the SSL flow and the WW flow. In the ideal case, the spanwise velocities would be matched. However, at the wall, $\tilde{w}_{\mathrm{s}}^{+\mathrm{s}} \neq 0$, whereas $\tilde{w}_{\mathrm{w}}^{+\mathrm{w}} = 0$ at the wall, which means we cannot possibly match the spanwise velocity profiles. So instead, they recognised that due to Galilean invariance, having similar motions in a different translated frame of reference will likely produce similar results. Therefore, instead the presumption was that having the same spanwise shear might affect turbulence the same way, leading to drag reduction. Thus, Chernyshenko [28] sought to match the SSL spanwise shear profile $\frac{\mathrm{d}\tilde{w}_{\mathrm{s}}^{+\mathrm{s}}}{\mathrm{d}y^{+\mathrm{s}}} = \hat{W}_{\mathrm{s}}^{+\mathrm{s}}\frac{\mathrm{d}\breve{w}_{\mathrm{s}}^{+\mathrm{s}}}{\mathrm{d}\breve{y}^{+\mathrm{s}}}e^{ik_x^{+\mathrm{s}}x^{+\mathrm{s}}}$ which is equivalent with $\frac{\mathrm{d}\tilde{w}_{\mathrm{s}}^{+0}}{\mathrm{d}y^{+0}} = \hat{W}_{\mathrm{s}}^{+0}\frac{\mathrm{d}\breve{w}_{\mathrm{s}}^{+0}}{\mathrm{d}\breve{y}^{+0}}e^{ik_x^{+0}x^{+0}}$ the WW spanwise shear profile $\frac{\mathrm{d}\tilde{w}_{\mathrm{w}}^{+\mathrm{w}}}{\mathrm{d}y^{+\mathrm{s}}} = ik_z^{+\mathrm{w}}\left(k_x^{+\mathrm{w}}\right)^{-2/3}\hat{P}_{\mathrm{w}}^{+\mathrm{w}}\frac{\mathrm{d}\breve{w}_{\mathrm{w}}^{+\mathrm{w}}}{\mathrm{d}\breve{y}^{+\mathrm{w}}}e^{i\left(k_x^{+\mathrm{w}}x + k_z^{+\mathrm{w}}z\right)}$. (———————————————) Dependence on z was neglected since $k_z^{+\mathrm{w}}$ for the WW is expected to be much larger than the characteristic scale of near wall turbulence. We know that streak spacing is around 100 wall units and their streamwise length is around 1000 wall units [43]; whereas the spanwise and streamwise wavelengths are expected to be on the same order, which from the

SSL analysis in Section 1.2.1 based on Viotti et al. [10] is expected to be around 1000 wall units for optimal performance. On the contrary, a phase shift ϕ could be added between the SSL spanwise shear profile and that of the WW, as it would still produce the necessary profiles just further down the flow in the streamwise direction, since the thickness of the Stokes layer and the WW boundary layer are much smaller than the channel half-height [41]. Therefore, matching the spanwise shear profiles with a phase shift is equivalent to minimising the following equation

$$\min\left\{\int_0^\infty \int_0^{\frac{2\pi}{k_x^+}} \left| \frac{\mathrm{d}\breve{w}_{\mathrm{s}}^{+\mathrm{s}}}{\mathrm{d}\breve{y}^{+\mathrm{s}}} e^{ik_x^{+\mathrm{s}}x^{+\mathrm{s}}} - \frac{ik_z^{+\mathrm{w}}\left(k_x^{+\mathrm{w}}\right)^{-2/3}\hat{P}_{\mathrm{w}}^{+\mathrm{w}}}{\hat{W}_{\mathrm{s}}^{+\mathrm{s}}} \frac{\mathrm{d}\breve{w}_{\mathrm{w}}^{+\mathrm{w}}}{\mathrm{d}\breve{y}^{+\mathrm{w}}} e^{i\left(k_x^{+\mathrm{w}}x^{+\mathrm{w}}+\phi\right)} \right|^2 \mathrm{d}x^+ \, \mathrm{d}y^+ \right\} \quad (1.54)$$

over $C = \frac{ik_z^{+\mathrm{w}}\left(k_x^{+\mathrm{w}}\right)^{-2/3}\hat{P}_{\mathrm{w}}^{+\mathrm{w}}}{\hat{W}_{\mathrm{s}}^{+\mathrm{s}}}$ and ϕ. Minimisation gave $C_{\min} = 0.8980$ and $\phi_{\min} = 1.5708$, which is (interestingly) approximately $\frac{\pi}{2}$. Thus, to match the spanwise shear profiles, the amplitude of the periodic pressure field should be such that

$$\hat{P}_{\mathrm{w}}^{+\mathrm{w}} = C_{\min} \frac{\hat{W}_{\mathrm{s}}^{+\mathrm{s}}}{ik_z^{+\mathrm{w}}\left(k_x^{+\mathrm{w}}\right)^{-2/3}}. \quad (1.55)$$

Note that the WW height is unknown a priori, therefore it is likely that it would have to be picked by guessing, and trial and error via DNS, Reynolds Averaged Navier-Stokes (RANS) simulations, or experiments to match the above periodic pressure field amplitude. The resulting spanwise shear-profile matching and its corresponding spanwise velocity are shown in Figures 1.8(a) and 1.8(b) respectively.

Net Power Reduction for WW

Similar to the SSL flow discussed in Section 1.2.1, we will define the net power reduction as a percentage of the power required to drive the reference channel flow as

$$P_{\mathrm{net,w}} \equiv P_{\mathrm{sav,w}} + P_{\mathrm{req,w}} \quad (1.56)$$

$$\equiv 100\% \frac{\Delta\Phi_{\overline{U},\mathrm{w}}^{+0} + \Delta\Phi_{\mathbf{u}',\mathrm{w}}^{+0}}{\Phi_0^{+0}} + 100\% \frac{\Delta\Phi_{\tilde{\mathbf{u}},\mathrm{w}}^{+0}}{\Phi_0^{+0}}, \quad (1.57)$$

where $\Delta\Phi_{\overline{U},\mathrm{w}}^{+0} = \Phi_{\overline{U},0}^{+0} - \Phi_{\overline{U},\mathrm{w}}^{+0}$, $\Delta\Phi_{\mathbf{u}',\mathrm{w}}^{+0} = \Phi_{\mathbf{u}',0}^{+0} - \Phi_{\mathbf{u}',\mathrm{w}}^{+0}$, and unlike SSL, with two phase averaged components $\Delta\Phi_{\tilde{\mathbf{u}},\mathrm{w}} = -\left(\Phi_{\tilde{u},\mathrm{w}} + \Phi_{\tilde{w},\mathrm{w}}\right)$. Unlike SSL, P_{req} is no longer the power required for the actuator to create the spanwise forcing, but is instead the extra power required by the hypothetical pump driving the main flow to overcome the phase averaged forcing in both the streamwise direction and the spanwise direction, the latter of which we have previously attempted to match to SSL as closely as possible.

Armed with the definition, it is known that at high Reynolds numbers, the differences in $\overline{U}^+$ is negligible. Therefore, in Chernyshenko [28], without even mentioning it specifically, it was assumed that the difference in mean velocity profiles between the reference and controlled flows were the same, i.e. $\Delta\Phi_{\overline{U},\mathrm{w}} = \Delta\Phi_{\overline{U},\mathrm{s}}$. Moreover, because of the matching of spanwise shear, it is therefore assumed that the effects on the stochastic turbulence leading to drag reduction is the same and therefore that $\Delta\Phi_{\mathbf{u}',\mathrm{w}} = \Delta\Phi_{\mathbf{u}',\mathrm{s}}$. Therefore, Chernyshenko [28] claimed that

$$P_{\mathrm{sav,w}} = P_{\mathrm{sav,s}}. \quad (1.58)$$

21
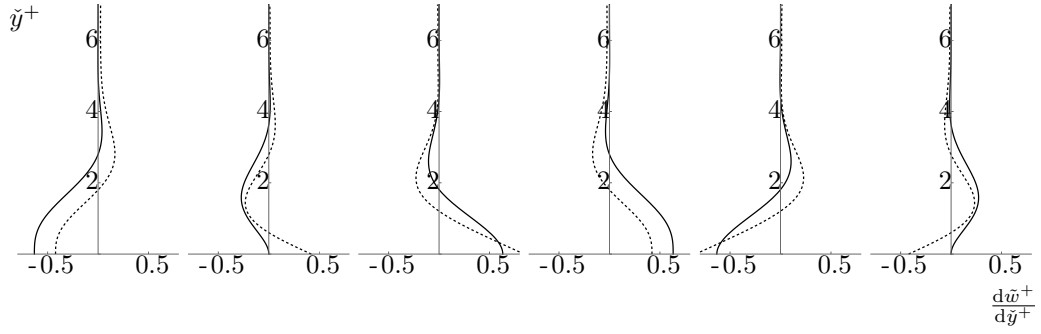
(a) Spanwise shear profiles.
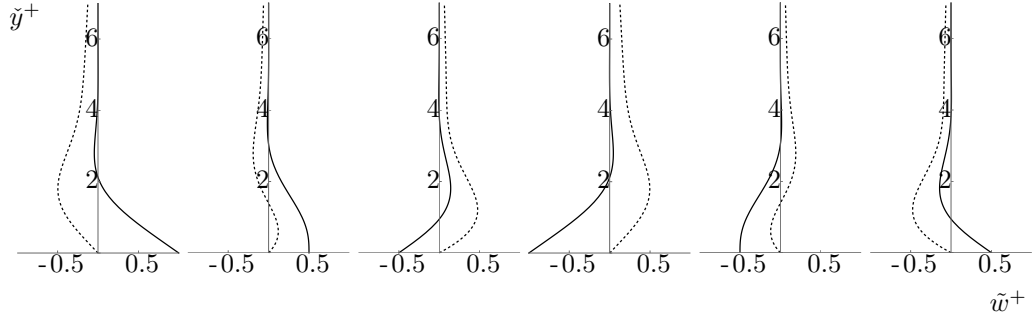
(b) Spanwise velocity profiles.

Figure 1.8: Spanwise shear (a) and velocity (b) profile comparison between SSL (solid) and WW (dashed) using $\mathrm{Re}\left\{\check{w}_{\mathrm{s}}^{+\mathrm{s}}(\check{y}^{+\mathrm{s}})e^{ik_x^{+\mathrm{s}}x^{+\mathrm{s}}}\right\}$ and $\mathrm{Re}\left\{C_{\min}\check{w}_{\mathrm{w}}^{+\mathrm{w}}(\check{y}^{+\mathrm{w}})e^{ik_x^{+\mathrm{w}}x^{+\mathrm{w}}}\right\}$ respectively for velocity, and their derivatives with respect to $\check{y}^+$ for shear at $\frac{k_x^+x^+}{2\pi}=0,\frac{1}{6},\frac{2}{6},\frac{3}{6},\frac{4}{6}$, and $\frac{5}{6}$ from left to right.

However, we do expect some change in the net power usage due to the presence of changing pressure gradients. The difference in power reduction, therefore, comes in the $P_{\mathrm{req,w}}$ term. For a wavy wall the dissipation due to phase averaged velocity gradients are given by (——————————————————————————————-sdakf ————————————————————————safkl idk———————————————-)

Thus,

$$\Phi_{\tilde{u},\mathrm{w}}^{+\mathrm{w}} = \int_0^\infty \overline{\left(\frac{\mathrm{d}\tilde{u}_{\mathrm{w}}^{+\mathrm{w}}}{\mathrm{d}y^{+\mathrm{w}}}\right)^2} \, \mathrm{d}y^{+\mathrm{w}} \tag{1.59}$$

$$= \int_0^\infty \left(\frac{\mathrm{d}i\left(k_z^{+\mathrm{w}}\right)^2 \left(k_x^{+\mathrm{w}}\right)^{-5/3} \hat{P}_{\mathrm{w}}^{+\mathrm{w}} \check{u}_{\mathrm{w}}^{+\mathrm{w}} e^{i\left(k_x^{+\mathrm{w}}x^{+\mathrm{w}}+k_z^{+\mathrm{w}}z^{+\mathrm{w}}\right)}}{\mathrm{d}\left((k_x^{+\mathrm{w}})^{-1/3}\check{y}^{+\mathrm{w}}\right)}\right)^2 \mathrm{d}\left((k_x^{+\mathrm{w}})^{-1/3}\check{y}^{+\mathrm{w}}\right) \tag{1.60}$$

$$= \left(k_z^{+\mathrm{w}}\right)^4 \left(k_x^{+\mathrm{w}}\right)^{-3} \hat{P}_{\mathrm{w}}^{+\mathrm{w}} \int_0^\infty \frac{1}{2}\left|\frac{\mathrm{d}\check{u}_{\mathrm{w}}^{+\mathrm{w}}}{\mathrm{d}\check{y}^{+\mathrm{w}}}\right|^2 \mathrm{d}\check{y}^{+\mathrm{w}} . \tag{1.61}$$

$$\Phi_{\tilde{w},\mathrm{w}}^{+\mathrm{w}} = \int_0^\infty \overline{\left(\frac{\mathrm{d}\tilde{w}_{\mathrm{w}}^{+\mathrm{w}}}{\mathrm{d}y^{+\mathrm{w}}}\right)^2} \, \mathrm{d}y^{+\mathrm{w}} \tag{1.62}$$

$$= \int_0^\infty \left(\frac{\mathrm{d}ik_z^{+\mathrm{w}}\left(k_x^{+\mathrm{w}}\right)^{-2/3} \hat{P}_{\mathrm{w}}^{+\mathrm{w}} \check{w}_{\mathrm{w}}^{+\mathrm{w}} e^{i\left(k_x^{+\mathrm{w}}x^{+\mathrm{w}}+k_z^{+\mathrm{w}}z^{+\mathrm{w}}\right)}}{\mathrm{d}\left((k_x^{+\mathrm{w}})^{-1/3}\check{y}^{+\mathrm{w}}\right)}\right)^2 \mathrm{d}\left((k_x^{+\mathrm{w}})^{-1/3}\check{y}^{+\mathrm{w}}\right) \tag{1.63}$$

$$= \left(k_z^{+\mathrm{w}}\right)^2 \left(k_x^{+\mathrm{w}}\right) \hat{P}_{\mathrm{w}}^{+\mathrm{w}} \int_0^\infty \frac{1}{2}\left|\frac{\mathrm{d}\check{w}_{\mathrm{w}}^{+\mathrm{w}}}{\mathrm{d}\check{y}^{+\mathrm{w}}}\right|^2 \mathrm{d}\check{y}^{+\mathrm{w}} . \tag{1.64}$$

By selecting $\hat{P}_{\mathrm{w}}^{+\mathrm{w}}$ using Equation (1.55), we are guaranteeing that $\Phi_{\tilde{w},\mathrm{w}}^{+\mathrm{w}} \leq \Phi_{\tilde{w},\mathrm{s}}^{+\mathrm{s}}$. This is because by optimising over C in Equation (1.54) "is equivalent to projecting the SSL solution onto the direction of the wavy-wall solution in the L_2 functional space" [28], i.e. it is equivalent to projecting the SSL spanwise shear profile as a vector in the direction of that of WW, which is necessarily equal or less than the magnitude of the SSL vector. To be safe in their calculations, Chernyshenko [28] therefore assumed the maximum value of $\Phi_{\tilde{w},\mathrm{s^{+s}}}^{+0}$ which is equal to $\Phi_{\tilde{w},\mathrm{s}}^{+0}$. Thus,

$$P_{\mathrm{req,w}} = 100\% \frac{-\left(\Phi_{\tilde{u},\mathrm{w}}^{+0} + \Phi_{\tilde{w},\mathrm{w}}^{+0}\right)}{\Phi_0^{+0}} = -100\% \frac{\Phi_{\tilde{u},\mathrm{w}}^{+0} + \Phi_{\tilde{w},\mathrm{w}}^{+0}}{\Phi_{\tilde{w},\mathrm{w}}^{+0}} \frac{\Phi_{\tilde{w},\mathrm{s}}^{+0}}{\Phi_0^{+0}} = \frac{\Phi_{\tilde{u},\mathrm{w}}^{+\mathrm{w}} + \Phi_{\tilde{w},\mathrm{w}}^{+\mathrm{w}}}{\Phi_{\tilde{w},\mathrm{w}}^{+\mathrm{w}}} P_{\mathrm{req,s}}. \tag{1.65}$$

Defining the squared norm $\|\cdot\|^2 \equiv \int_0^\infty (\cdot)^2 \, \mathrm{d}y$, we can define a ratio r as follows

$$r \equiv \frac{\Phi_{\tilde{u},\mathrm{w}}^{+\mathrm{w}} + \Phi_{\tilde{w},\mathrm{w}}^{+\mathrm{w}}}{\Phi_{\tilde{w},\mathrm{w}}^{+\mathrm{w}}} = \frac{\|\hat{W}_{\mathrm{w}}^{+\mathrm{w}}\|^2 + \|\hat{U}_{\mathrm{w}}^{+\mathrm{w}}\|^2}{\|\hat{W}_{\mathrm{w}}^{+\mathrm{w}}\|^2} = 1 + \left(\frac{k_x^{+\mathrm{w}}}{k_z^{+\mathrm{w}}}\right)^{-2} \frac{\|\check{u}_{w,\mathrm{w}}^{+\mathrm{w}} + \left(\frac{k_x^{+\mathrm{w}}}{k_z^{+\mathrm{w}}}\right)^2 \check{u}_{p,\mathrm{w}}^{+\mathrm{w}}\|^2}{\|\check{w}_{\mathrm{w}}^{+\mathrm{w}}\|^2}. \tag{1.66}$$

Since they are fractions, the non-dimensionalisation by wall units here is unnecessary but included for clarity. r, as it turns out, is only dependent on $\frac{k_x^{+\mathrm{w}}}{k_z^{+\mathrm{w}}}$; numerically determining the norms, it was found that

$$r = 3.122 + 2.323\left(\frac{k_x^{+\mathrm{w}}}{k_z^{+\mathrm{w}}}\right)^2 + 0.7986\left(\frac{k_x^{+\mathrm{w}}}{k_z^{+\mathrm{w}}}\right)^{-2}. \tag{1.67}$$

By minimising r, we minimise $P_{\mathrm{req,w}}$. This is given by

$$r_{\min} = 5.846 \text{ at } \frac{k_x^{+\mathrm{w}}}{k_z^{+\mathrm{w}}}\big|_{\mathrm{opt}} = 0.7657 \implies \theta_{\mathrm{opt}} = 52.56°, \tag{1.68}$$

where θ_{opt} is the optimal oblique angle of the WW to the streamwise direction.

Finally, with $P_{\mathrm{net,w}} = P_{\mathrm{sav,w}} + P_{\mathrm{req,w}} = P_{\mathrm{sav,s}} + rP_{\mathrm{req,s}}$, and the known results of the latter three terms from this section and Section 1.2.1, we can estimate the net power reduction of th WW flow as compared to the reference flow. This is plotted in Figure 1.5 for the prescribe $\hat{W}_{\mathrm{s}}^{+0} = 2, 6$ for $P_{\mathrm{sav,w}} = P_{\mathrm{sav,s}}$. It was shown that $\hat{W}_{\mathrm{s}}^{+0} = 2$ gives the best result at $\lambda_x^{+0} = 1520$ of a net power savings due to drag reduction of 2.4% compared to the reference flow. Moreover, DNS of the flow at $Re_\tau \approx 180$ at approximately these optimal conditions gave $r = 5.4$ [42], which is similar to that we found as r_{min}.

1.2.3 CFD Results of the Wavy Wall (WW)

Ghebali et al. [41] performed DNS of the WW at $Re_\tau \approx 360$, which is incredibly computationally expensive as it requires a large domain, especially since the domain now has to accommodate for the spanwise wavelength of the WW, which is an order of magnitude larger than the spanwise spacing of streaks [43]. This means that only a few configurations were tested, and that so-far this is the only detailed numerical simulation of the WW. The change in Re_τ as compared to that of Viotti et al. [10], which used $Re_\tau = 200$, is assumed to not have significant impact on the optimal wavelength [41]. Strangely, they found that as mesh size of the domain is refined, the predicted drag reduction decreases. The maximum net drag reduction was found to be 0.7% with a 2% friction drag reduction and 1.3% pressure drag penalty, at a configuration of wall height amplitude $\alpha^{+\mathrm{w}} \approx 20$, WW angle $\theta = 70°$, and WW streamwise wavelength $\lambda_x^{+\mathrm{w}} \approx 920$ [41]. Although it "appears to tend, asymptotically to a positive value of 0.6%" under the configuration of [41]. Higher friction drag reduction by increasing height amplitude is possible, but comes at a great cost of pressure drag. van Nesselrooij et al. [44] showed that dimpled surfaces for drag reduction cannot be too high as separation occurs, what's more is that the adverse pressure gradient becomes stronger, which generates instabilities via different mechanisms therefore changing the total drag reduction. (————————————no citation——————————————————)This value of 0.6% was therefore thought to be the maximum possible net drag reduction, which is significantly lower than the 2.4% predicted by Chernyshenko [28] with a different θ.

This discrepancy is believed to have potentially come from the assumption that $P_{\mathrm{sav,w}} = P_{\mathrm{sav,s}}$. Gatti and Quadrio [45] examined the effects of Reynolds number on turbulent skin-friction drag reduction using spanwise forcing. They found that at low Reynolds numbers, $Re_\tau \approx 200$, which is the regime for which these analyses were conducted, the vertical shift of the logarithmic portion of the mean streamwise velocity profile did not stay constant. Therefore, it is believed that the assumption that $\overline{U}_{\mathrm{w}}^{+\mathrm{w}} = \overline{U}_{\mathrm{s}}^{+\mathrm{s}}$ is in fact untrue, and therefore the resulting change in dissipation due to the mean profile is also false.

1.3 Problem Formulation

The main objective of this project is to be able to predict an estimate of the net drag reduction (DR) due to the wavy wall (WW) for a given wavy wall prescribed by k_x^{+0}, k_z^{+0}, and the corresponding $\hat{W}_s^{+0}$ at $Re_\tau = 200$ using only the curve fitted to $P_{\text{sav,s}}$ DNS data from Viotti et al. [10]. A first attempt at this objective was already done by Chernyshenko [28], and relayed again in Section 1.2.2 of this report. However, as outlined in Section 1.2.3, we believe there was an error in the assumptions made; in that at these low Reynolds numbers the changes in dissipation due to mean streamwise velocity profile between two similar flows cannot be ignored. This report will therefore show our attempts to take the changes into account.

To do so (——————————— sections 1, 2, 3————-)

Chapter 2

Project - Wavy Wall Analysis

2.1 Power Saved by the Wavy Wall (WW)

With our definition of $P_{\mathrm{sav,w}}$ staying the same, we no longer believe it is equal to $P_{\mathrm{sav,s}}$. However, since we matched the periodic spanwise shear, we still maintain that the reduction in stochastic turbulent dissipation is the same between the wavy wall (WW) and spatial Stokes layer (SSL) flow, i.e. $\frac{\Delta\Phi_{\mathbf{u}',\mathrm{s}}^{+0}}{\Phi_0^{+0}} = \frac{\Delta\Phi_{\mathbf{u}',\mathrm{w}}^{+0}}{\Phi_0^{+0}}$. Therefore,

$$P_{\mathrm{sav,w}} - P_{\mathrm{sav,s}} = 100\% \frac{\Delta\Phi_{\overline{U},\mathrm{w}}^{+0} + \Delta\Phi_{\mathbf{u}',\mathrm{w}}^{+0}}{\Phi_0^{+0}} - 100\% \frac{\Delta\Phi_{\overline{U},\mathrm{s}}^{+0} + \Delta\Phi_{\mathbf{u}',\mathrm{s}}^{+0}}{\Phi_0^{+0}} \tag{2.1}$$

$$P_{\mathrm{sav,w}} - P_{\mathrm{sav,s}} = 100\% \frac{\Delta\Phi_{\overline{U},\mathrm{w}}^{+0} - \Delta\Phi_{\overline{U},\mathrm{s}}^{+0}}{\Phi_0^{+0}} \tag{2.2}$$

$$P_{\mathrm{sav,w}} = 100\% \frac{\Phi_{\overline{U},\mathrm{w}}^{+0} - \Phi_{\overline{U},\mathrm{s}}^{+0}}{\Phi_0^{+0}} + P_{\mathrm{sav,s}}. \tag{2.3}$$

2.2 The Spatial Stokes Layer (SSL) Mean Velocity Profile

Since we do not know the shape of the WW mean streamwise velocity profile to figure out dissipation due to the mean profile, we must start elsewhere. The SSL mean streamwise velocity profile $\overline{U}_{\mathrm{s}}^{+\mathrm{s}}$ was given by Viotti et al. [10], along with that of temporal Stokes layer (TSL), the reference channel flow, and $\overline{U}^+ = y^+$ for comparison (Figure 2.1). We can see that at $y^+ < 10$, they all coincide to the linear profile $\overline{U}^+ = y^+$, and at some point between $10 < y^+ < 40$, they stop being curved on the logarithmic plot and become straight with similar slopes, indicating a logarithmic profile at higher y^+. In fact, like other drag reduction (DR) techniques (e.g. riblets), the DR is noticeable as a thickening of the viscous sublayer causing an upward shift in this logarithmic portion of the mean velocity profile [10, 46, 47].

In order to see the differences more clearly, the SSL and refence flow data from Figure 2.1 were digitised using the web app webplotdigitiser. Then a curve fit was implemented and plotted in Figure 2.2(a) using an analytical fit for a turbulent plane channel flows given in an unpublished
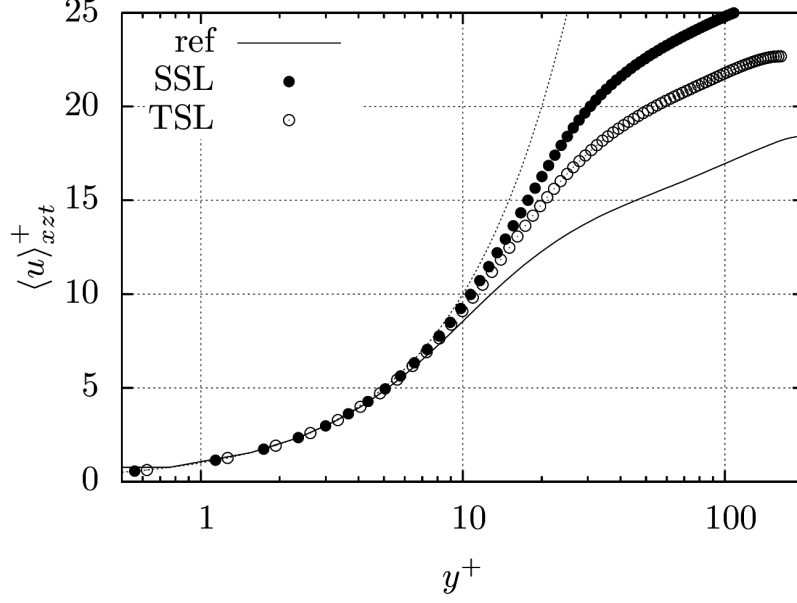
Figure 2.1: Streamwise mean velocity profiles in wall units averaged in x-z space, time, and phase $(\overline{U}^+ \equiv \langle u \rangle_{xzt}^+)$ for SSL, TSL, the reference flow, and $\overline{U}^+ = y^+$ (dotted line) for comparison [10].

supplement to [48]. Abnormally, though, when the curve fit given for the mean streamwise velocity was used, the derivative thereof fluctuated much more than expected. Therefore, the curve fit for the second moments of velocity near the wall (root mean square velocity) was trialled instead, which produced much more reasonable derivative whilst also maintaining a good curve fit in and of itself. This latter curve fit is given as

$$y^+ \frac{a\left(y^+\right)^2 + by^+ + c}{q\left(y^+\right)^2 + ry^+ + 1} + p\left(\ln\left(y^+ + 15\right) - \ln(15)\right), \tag{2.4}$$

where a, b, c, p, q, r are some coefficients. This function, however, does not guarantee that $\frac{\mathrm{d}U^+}{\mathrm{d}y^+} = 1$ at the wall, which would be most accurate. We can see again that at $y^+ < 10$, the curves both fit on the $\overline{U}^+ = y^+$ line. Then there is an area where the two curves diverge, but then, at around $y^+ > 60$, the gradients $\frac{\mathrm{d}\overline{U}^+}{\mathrm{d}y^+}$ seem to look fairly similar and in fact become negligible. This, as Viotti et al. [10] had done, lead us to conjecture that the logarithmic portion of the SSL mean velocity profile was the same as that of the reference flow but with an extra vertical shift.

Therefore, we take the well known logarithmic portion of the law of the wall, which applies to the reference flow,

$$\overline{U}_0^{+0} = \frac{1}{\kappa} \ln y^{+0} + B, \tag{2.5}$$

where $\kappa = 0.41$, and $B = 5.0$ [29], and add a vertical shift Δh to get

$$\overline{U}_{\mathrm{s}}^{+\mathrm{s}} = \frac{1}{\kappa} \ln y^{+\mathrm{s}} + B + \Delta h_{\mathrm{s}}. \tag{2.6}$$

Δh can easily be estimated by drawing a straight line that follows the logarithmic portion of the SSL mean profile (where $y^+ > 60$) on the logarithmic scale (in Figure 2.1), reading the intercept of said straight line, and subtracting by B. By this method it was found that $\Delta h \approx 8$. Curve fits using Equations (2.5) and (2.6) are plotted in Figure 2.2(b).

(a) Curve fits.

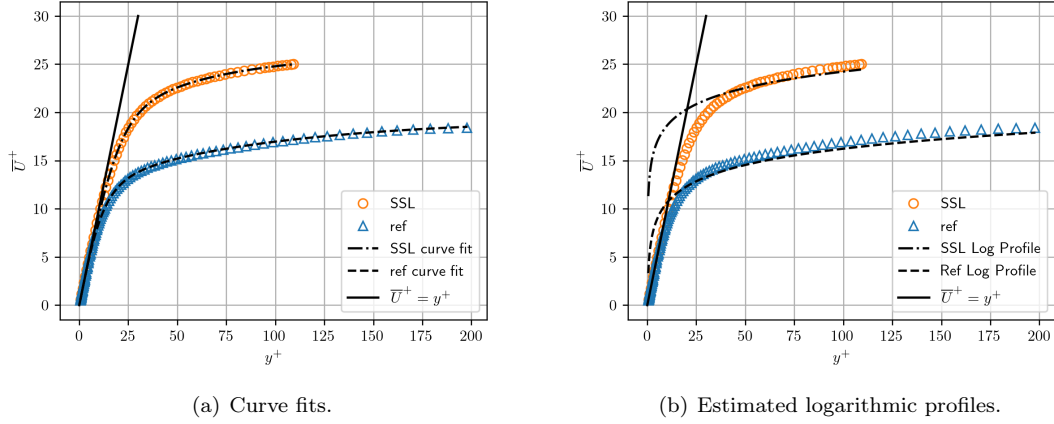(b) Estimated logarithmic profiles.

Figure 2.2: Both plots show data on the mean streamwise velocity profiles of SSL (orange-circle) and the reference flow (blue-triangles) which were digitised from Viotti et al. [10] (shown in Figure 2.1 and plotted on a linear scale, as well as $\overline{U}^+ = y^+$ (solid-line).

The validity of using the same logarithmic profile with vertical shift as an estimate can be further seen in Figure 2.3, where the squares of the derivatives of the curvefits found using Equation (2.4) were plotted for the SSL and reference flows. We can see that the differences in the derivatives are negligibly small. Moreover, since dissipation is equal to the integral of this derivative from 0 to infinity, we can see that contributions at $y^+ > 60$ are negligible. Whilst we can only numerically integrate the curve fitted solution, we can actually analytically integrate the estimated solution as

$$\Phi_{\overline{U}}^+ = \int_0^{y_\times^+} \left| \frac{dy^+}{dy^+} \right|^2 dy^+ + \int_{y_\times^+}^\infty \left| \frac{d\left(\frac{1}{\kappa}\ln y^+ + B + \Delta h\right)}{dy^+} \right|^2 dy^+ \tag{2.7}$$

$$= \int_0^{y_\times^+} 1 \, dy^+ + \frac{1}{\kappa^2} \int_{y_\times^+}^\infty \left| \frac{1}{y^+} \right|^2 dy^+ \tag{2.8}$$

$$= y_\times^+ + \frac{1}{\kappa^2} \frac{1}{y_\times^+} \tag{2.9}$$

$$= \frac{\left(\kappa y_\times^+\right)^2 + 1}{\kappa^2 y_\times^+}, \tag{2.10}$$

where $y_\times^+$ is the single point at which the linear profile crosses the logarithmic profile. For SSL, we have We find that for this estimated profile, the ratio $\frac{\Phi_{\overline{U},s}^{+s}}{\Phi_{\overline{U},0}^{+0}}|_{\text{est}} = 1.818$, whereas the same ratio for the curve fitted profile $\frac{\Phi_{\overline{U},s}^{+s}}{\Phi_{\overline{U},0}^{+0}}|_{\text{cfit}} = 1.650$. The estimated ratio is only 10.1% higher than that of the curve fitted solution. Therefore, the idea is that perhaps if we could model the mean profile of the WW using the linear plus logarithmic profile approach, perhaps it would be good enough to measure the net power reduction of the WW flow.
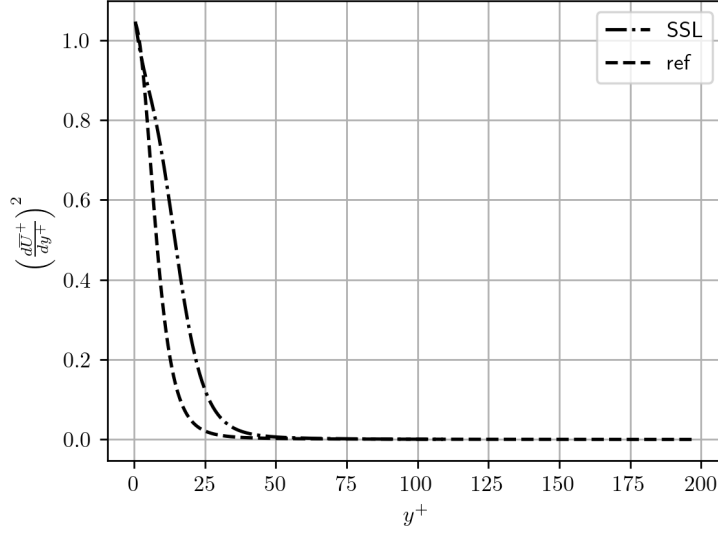
Figure 2.3: The squared mean streamwise shear profiles of SSL (dot-dash), and reference (dash) flows, i.e. the squared derivative of mean streamwise velocity profiles $\frac{\mathrm{d}\overline{U}^+}{\mathrm{d}y^+}$ obtained using Equation (2.4) for $\overline{U}^+$, which is shown in Figure 2.2(a).

2.3   Modelling the Wavy Wall (WW) Mean Velocity Profile

With Equation (2.6), Luchini [47] wrote that "an increment in [B i.e. Δh] can be quantitatively translated into drag reduction because [B] appears explicitly in the drag formulae that" since we can just integrate the mean velocity profile. For a turbulent boundary layer over a flat plate, the friction formula is given by

$$\left(\frac{C_f}{2}\right)^{-1/2} = \frac{1}{\kappa} \ln\left[\left(\frac{C_f}{2}\right)^{1/2} Re_D\right] + 2.2 + B, \tag{2.11}$$

where Re_D is based on the velocity boundary-layer thickness [49]. It turns out that for small increments in B,

$$\frac{\Delta C_f}{C_{f,0}} = -\frac{\Delta h}{(2C_{f,0})^{-1/2} + \kappa/2}, \tag{2.12}$$

where $\Delta C_f = C_f - C_{f,0}$ [47]. For WW, $P_{\mathrm{net,w}} \equiv 100\%\frac{C_{f,0}-C_{f,\mathrm{w}}}{C_{f,0}}$. Therefore,

$$-\frac{P_{\mathrm{net,w}}}{100\%} = -\frac{\Delta h_{\mathrm{w}}}{(2C_{f,0})^{-1/2} + \kappa/2} \tag{2.13}$$

$$\Delta h_{\mathrm{w}} = \frac{P_{\mathrm{net,w}}}{100\%\left[(2C_{f,0})^{-1/2} + \kappa/2\right]}. \tag{2.14}$$

Thus, we believe the WW mean velocity profile can be modelled by

$$\overline{U}_{\mathrm{w}}^{+\mathrm{w}} = \begin{cases} y^{+\mathrm{w}}, & y^{+\mathrm{w}} \leq y_{\times}^{+\mathrm{w}} \\ \frac{1}{\kappa}\ln y^{+\mathrm{w}} + B + \frac{P_{\mathrm{net,w}}}{100\%\left[(2C_{f,0})^{-1/2}+\kappa/2\right]}, & y^{+\mathrm{w}} > y_{\times}^{+\mathrm{w}} \end{cases}. \tag{2.15}$$

By modelling the WW mean velocity profile like so, we can find $P_{\mathrm{net,w}}$ as only a function of $y_{\times}^{+\mathrm{w}}$ by solving the two cases as a system of equations, i.e. we let $\overline{U}_{\mathrm{w}}^{+\mathrm{w}} = y^{+\mathrm{w}}$ in the logarithmic

profile as follows

$$\overline{U}_{\text{w}}^{+\text{w}} = \frac{1}{\kappa} \ln y^{+\text{w}} + B + \frac{P_{\text{net,w}}}{100\% \left[(2C_{f,0})^{-1/2} + \kappa/2\right]} \tag{2.16}$$

$$y_{\times}^{+\text{w}} = \frac{1}{\kappa} \ln y_{\times}^{+\text{w}} + B + \frac{P_{\text{net,w}}}{100\% \left[(2C_{f,0})^{-1/2} + \kappa/2\right]} \tag{2.17}$$

$$P_{\text{net,w}} = 100 \left(y_{\times}^{+\text{w}} - \frac{1}{\kappa} \ln y_{\times}^{+\text{w}} - A \right) \left((2C_{f,0})^{-\frac{1}{2}} + \frac{\kappa}{2} \right). \tag{2.18}$$

Moreover, we can also employ Equation (2.10) combined with the wall unit conversions just as Equation (1.30) to get

$$\Phi_{\overline{U},\text{w}}^{+0} = \Phi_{\overline{U},\text{w}}^{+\text{w}} \left(\frac{\tau_{w,\text{w}}}{\tau_{w,0}} \right)^{3/2} = \frac{\left(\kappa y_{\times}^{+}\right)^2 + 1}{\kappa^2 y_{\times}^{+}} \left(\frac{\tau_{w,\text{w}}}{\tau_{w,0}} \right)^{3/2}. \tag{2.19}$$

But there is a slight problem here. Previously, for $\frac{\tau_{w,\text{s}}}{\tau_{w,0}}$, we have simply said this is equal to $1 - \frac{P_{\text{sav,s}}}{100\%}$ in an SSL flow. However, in a WW flow, this is not necessarily the case. τ_w only involves the frictional drag of the flow (the wall shear stress), but leaves out pressure drag which is present in the WW due to the undulations which create pressure gradients. As of writing, the author knows of no way to extract $\frac{\tau_{w,\text{w}}}{\tau_{w,0}}$. The only solution was to turn to direct numerical simulation (DNS) by Ghebali et al. [41]. Through their results we were able to find that although the drag reduction and pressure drag reduction were of the same order, the pressure drag reduction was at least an order of magnitude smaller than the total drag, i.e. we conjecture that pressure drag on the WW is $\ll \tau_{w,\text{w}}$. Therefore, we let

$$P_{\text{net,w}} \approx 100\% \frac{\tau_{w,0} - \tau_{w,\text{w}}}{\tau_{w,0}} \implies \frac{\tau_{w,\text{w}}}{\tau_{w,0}} \approx 1 - \frac{P_{\text{net,w}}}{100\%}, \tag{2.20}$$

even though it isn't necessarily true.

2.4 Net Power Reduction by Wavy Wall (WW) - Results

By accepting the assumption in Equation (2.20), quite accidentally, we have now stumbled upon a closed set of equations for which we can solve numerically for a given λ_x^{+0}, λ_z^{+0}, and $\hat{W}_{\text{s}}^{+0}$. We start by recognising that nowhere in our analysis did we need to involve $P_{\text{req,w}} = r_{\min} P_{\text{req,s}}$. Therefore,

$r_{\min}$ stays the same, and $\frac{\lambda_x^{+0}}{\lambda_z^{+0}}|_{\mathrm{opt}}$ stays the same. Thus the closed set of equations is as follows

$$P_{\mathrm{net,w}} = P_{\mathrm{sav,w}} + r_{\min} P_{\mathrm{req,s}} \tag{2.21}$$

$$P_{\mathrm{sav,w}} = 100\% \sqrt{\frac{C_{f,0}}{2} \left(\frac{\left(\kappa y_{\times,\mathrm{w}}^{+\mathrm{w}}\right)^2 + 1}{\kappa^2 y_{\times,\mathrm{w}}^{+\mathrm{w}}} \left(\frac{\tau_{w,\mathrm{w}}}{\tau_{w,0}}\right)^{\frac{3}{2}} - \Phi_{\overline{U},\mathrm{s}}^{+0} \right) + P_{\mathrm{sav,s}}} \tag{2.22}$$

$$P_{\mathrm{net,w}} = 100\% \left(y_{\times}^{+\mathrm{w}} - \frac{1}{\kappa} \ln y_{\times}^{+\mathrm{w}} - B \right) \left((2C_{f,0})^{-\frac{1}{2}} + \frac{\kappa}{2} \right) \tag{2.23}$$

$$P_{\mathrm{req,s}} = -100\% \left(\hat{W}^{+0}\right)^2 \sqrt{\frac{C_{f,0}}{2}} \left(\frac{2\pi(1 - P_{\mathrm{sav,s}}/100\%)}{\lambda_x^{+0}} \right)^{\frac{1}{3}} \int_0^\infty \frac{1}{2} \left| \frac{d\breve{w}_{\mathrm{s}}^{+\mathrm{s}}}{d\breve{y}^{+\mathrm{s}}} \right|^2 d\breve{y}^{+\mathrm{s}} \tag{2.24}$$

$$P_{\mathrm{sav,s}} = f\left(\lambda_x^{+0}, \hat{W}_{\mathrm{s}}^{+0}\right) \quad \text{(from Equation (1.27))} \tag{2.25}$$

$$\Phi_{\overline{U},\mathrm{s}}^{+0} = \left(1 - \frac{P_{\mathrm{sav,s}}}{100\%} \right) \left[\frac{\left(\kappa y_{\times,\mathrm{s}}^{+\mathrm{s}}\right)^2 + 1}{\kappa^2 y_{\times,\mathrm{s}}^{+\mathrm{s}}} \right] \tag{2.26}$$

$$y_{\times,\mathrm{s}}^{+\mathrm{s}} = \frac{1}{\kappa} \ln y_{\times,\mathrm{s}}^{+\mathrm{s}} + B + \Delta h_{\mathrm{s}} \tag{2.27}$$

$$C_{f,0} = 0.00336 Re_\tau^{-0.273}, \tag{2.28}$$

where $\Delta h_{\mathrm{s}} = 8$, $Re_\tau = 200$, $\kappa = 0.41$, $B = 5.0$, $r_{\min} = 5.846$, and $\int_0^\infty \frac{1}{2} \left| \frac{d\breve{w}_{\mathrm{s}}^{+\mathrm{s}}}{d\breve{y}^{+\mathrm{s}}} \right|^2 d\breve{y}^{+\mathrm{s}} = 0.3157$.

We solved this for $P_{\mathrm{net,w}}$ as a function of λ_x^{+0} for $\hat{W}_{\mathrm{s}}^{+0} = 1, 2, 6, 12$ and plotted them in Figure 2.4. The code for solving these equations, as well as others in this report, along with many of the figures generated is in Appendix A.
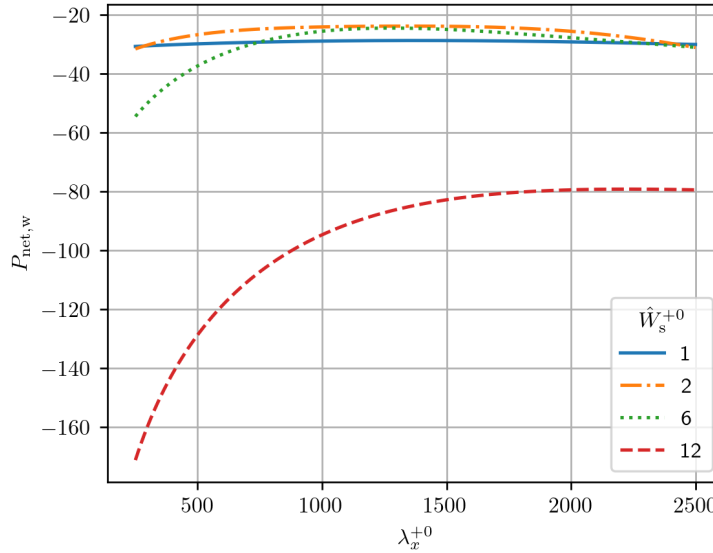

Figure 2.4: Calculated net power reduction $P_{\mathrm{net,w}}$ for the wavy wall $P_{\mathrm{net,w}}$.

Chapter 3

Conclusion

Code is broken

τ_w/τ_0 problem Ycross is enough to find Pnet Subject to (1) the closed system has been obtained

Wave height versus pressure

Although ideally, we would be able to predict from $h_w = \alpha \sin\left(k_x^{+\mathrm{w}} x + k_z^{+\mathrm{w}}\right)$

Bibliography

[1]   IEA. *Transport - Improving the Sustainability of Passenger and Freight Transport*. IEA. 2021. URL: https://www.iea.org/topics/transport (visited on 14/09/2021).

[2]   Mohamed Gad-el-Hak. 'Flow Control: The Future'. In: *Journal of Aircraft* 38.3 (2001), pp. 402–418. DOI: 10.2514/2.2796.

[3]   Ludwig Prandtl. 'Über Flüssigkeitsbewegung bei sehr kleiner Reibung'. In: *Proceedings of the Third International Mathematical Congress*. Proceedings of the Third International Mathematical Congress. Heidelberg, 8th–13th Aug. 1904, pp. 484–491.

[4]   Michael A. Leschziner, Haecheon Choi, and Kwing-So Choi. 'Flow-Control Approaches to Drag Reduction in Aerodynamics: Progress and Prospects'. In: *Philosophical Transactions of the Royal Society A: Mathematical, Physical and Engineering Sciences* 369.1940 (13th Apr. 2011), pp. 1349–1351. DOI: 10.1098/rsta.2010.0375.

[5]   Adel Abbas et al. 'Drag Reduction via Turbulent Boundary Layer Flow Control'. In: *Science China Technological Sciences* 60.9 (1st Sept. 2017), pp. 1281–1290. ISSN: 1869-1900. DOI: 10.1007/s11431-016-9013-6.

[6]   Haecheon Choi, Parviz Moin, and John Kim. 'Active Turbulence Control for Drag Reduction in Wall-Bounded Flows'. In: *Journal of Fluid Mechanics* 262 (1994), pp. 75–110. ISSN: 0022-1120. DOI: 10.1017/S0022112094000431.

[7]   M. Luhar, A. S. Sharma, and B. J. McKeon. 'Opposition Control within the Resolvent Analysis Framework'. In: *Journal of Fluid Mechanics* 749 (June 2014), pp. 597–626. ISSN: 0022-1120, 1469-7645. DOI: 10.1017/jfm.2014.209.

[8]   W. J. Jung, N. Mangiavacchi, and R. Akhavan. 'Suppression of Turbulence in Wall-bounded Flows by High-frequency Spanwise Oscillations'. In: *Physics of Fluids A: Fluid Dynamics* 4.8 (1st Aug. 1992), pp. 1605–1607. ISSN: 0899-8213. DOI: 10.1063/1.858381.

[9]   Kwing-So Choi, Jean-Robert DeBisschop, and Brian R. Clayton. 'Turbulent Boundary-Layer Control by Means of Spanwise-Wall Oscillation'. In: *AIAA Journal* 36.7 (1st July 1998), pp. 1157–1163. ISSN: 0001-1452. DOI: 10.2514/2.526.

[10] Claudio Viotti, Maurizio Quadrio, and Paolo Luchini. 'Streamwise Oscillation of Spanwise Velocity at the Wall of a Channel for Turbulent Drag Reduction'. In: *Physics of Fluids* 21.11 (Nov. 2009), p. 115109. ISSN: 1070-6631, 1089-7666. DOI: 10.1063/1.3266945.

[11] PanFeng Zhang, JinJun Wang, and LiHao Feng. 'Review of Zero-Net-Mass-Flux Jet and Its Application in Separation Flow Control'. In: *Science in China Series E: Technological Sciences* 51.9 (8th Aug. 2008), p. 1315. ISSN: 1862-281X. DOI: 10.1007/s11431-008-0174-x.

[12] Jin-Jun Wang et al. 'Recent Developments in DBD Plasma Flow Control'. In: *Progress in Aerospace Sciences* 62 (1st Oct. 2013), pp. 52–78. ISSN: 0376-0421. DOI: 10.1016/j.paerosci.2013.05.003.

[13] T. L. Chng et al. 'Flow Control of an Airfoil via Injection and Suction'. In: *Journal of Aircraft* 46.1 (1st Jan. 2009), pp. 291–300. DOI: 10.2514/1.38394.

[14] James Bird, Matthew Santer, and Jonathan F. Morrison. 'Experimental Control of Turbulent Boundary Layers with In-Plane Travelling Waves'. In: *Flow, Turbulence and Combustion* 100.4 (1st June 2018), pp. 1015–1035. ISSN: 1573-1987. DOI: 10.1007/s10494-018-9926-2.

[15] Paul K. Chang. 'CHAPTER XII - Control of Separation of Flow'. In: *Separation of Flow*. Ed. by Paul K. Chang. Pergamon, 1st Jan. 1970, pp. 716–752. ISBN: 978-0-08-013441-3. DOI: 10.1016/B978-0-08-013441-3.50016-2.

[16] K.–S. Choi et al. 'Turbulent Drag Reduction Using Compliant Surfaces'. In: *Proceedings of the Royal Society of London. Series A: Mathematical, Physical and Engineering Sciences* 453.1965 (8th Oct. 1997), pp. 2229–2240. DOI: 10.1098/rspa.1997.0119.

[17] Katharina Klausmann and Bodo Ruck. 'Drag Reduction of Circular Cylinders by Porous Coating on the Leeward Side'. In: *Journal of Fluid Mechanics* 813 (25th Feb. 2017), pp. 382–411. ISSN: 0022-1120, 1469-7645. DOI: 10.1017/jfm.2016.757.

[18] Richard Truesdell et al. 'Drag Reduction on a Patterned Superhydrophobic Surface'. In: *Physical Review Letters* 97.4 (26th July 2006), p. 044504. DOI: 10.1103/PhysRevLett.97.044504.

[19] Michael J. Walsh. 'Riblets as a Viscous Drag Reduction Technique'. In: *AIAA Journal* 21.4 (1983), pp. 485–486. ISSN: 0001-1452. DOI: 10.2514/3.60126.

[20] Haecheon Choi, Parviz Moin, and John Kim. 'Direct Numerical Simulation of Turbulent Flow over Riblets'. In: *Journal of Fluid Mechanics* 255 (Oct. 1993), pp. 503–539. ISSN: 1469-7645, 0022-1120. DOI: 10.1017/S0022112093002575.

[21] Ricardo García-Mayoral and Javier Jiménez. 'Drag Reduction by Riblets'. In: *Philosophical Transactions of the Royal Society A: Mathematical, Physical and Engineering Sciences* 369.1940 (13th Apr. 2011), pp. 1412–1427. DOI: 10.1098/rsta.2010.0359.

[22] Maurizio Quadrio, Pierre Ricco, and Claudio Viotti. 'Streamwise-Travelling Waves of Spanwise Wall Velocity for Turbulent Drag Reduction'. In: *Journal of Fluid Mechanics* 627 (May 2009), pp. 161–178. ISSN: 1469-7645, 0022-1120. DOI: 10.1017/S0022112009006077.

[23] J. R. Debisschop and F. T. M. Nieuwstadt. 'Turbulent Boundary Layer in an Adverse Pressure Gradient - Effectiveness of Riblets'. In: *AIAA Journal* 34.5 (1st May 1996), pp. 932–937. ISSN: 0001-1452. DOI: 10.2514/3.13170.

[24] E. Coustols and V. Schmitt. 'Synthesis of Experimental Riblet Studies in Transonic Conditions'. In: *Turbulence Control by Passive Means*. Ed. by E. Coustols. Fluid Mechanics and Its Applications. Dordrecht: Springer Netherlands, 1990, pp. 123–140. ISBN: 978-94-009-2159-7. DOI: 10.1007/978-94-009-2159-7_8.

[25] D.W. Bechert and W. Hage. 'Drag Reduction with Riblets in Nature and Engineering'. In: *WIT Transactions on State of the Art in Science and Engineering*. Ed. by R. Liebe. 1st ed. Vol. 2. WIT Press, 10th Nov. 2006, pp. 457–504. ISBN: 978-1-84564-095-8. DOI: 10.2495/1-84564-095-0/5g.

[26] J. Szodruch. 'Viscous Drag Reduction on Transport Aircraft'. In: *29th Aerospace Sciences Meeting*. Aerospace Sciences Meetings. American Institute of Aeronautics and Astronautics, 7th Jan. 1991. DOI: 10.2514/6.1991-685.

[27] Shabnam Raayai-Ardakani and Gareth H. McKinley. 'Geometric Optimization of Riblet-Textured Surfaces for Drag Reduction in Laminar Boundary Layer Flows'. In: *Physics of Fluids* 31.5 (May 2019), p. 053601. ISSN: 1070-6631, 1089-7666. DOI: 10.1063/1.5090881.

[28] Sergei Chernyshenko. *Drag Reduction by a Solid Wall Emulating Spanwise Oscillations. Part 1*. 16th Apr. 2013. arXiv: 1304.4638 [physics.flu-dyn]. URL: http://arxiv.org/abs/1304.4638 (visited on 10/09/2021).

[29] Hermann Schlichting and Klaus Gersten. *Boundary-Layer Theory*. Springer, 2016. ISBN: 3-662-52919-X.

[30] G.E. Karniadakis and Kwing-So Choi. 'Mechanisms on Transverse Motions in Turbulent Wall Flows'. In: *Annual Review of Fluid Mechanics* 35.1 (1st Jan. 2003), pp. 45–62. ISSN: 0066-4189. DOI: 10.1146/annurev.fluid.35.101101.161213.

[31] M. R. Dhanak and C. Si. 'On Reduction of Turbulent Wall Friction through Spanwise Wall Oscillations'. In: *Journal of Fluid Mechanics* 383 (1999), pp. 175–195. ISSN: 0022-1120. DOI: 10.1017/S0022112098003784.

[32] Arturo Baron and Maurizio Quadrio. 'Turbulent Drag Reduction by Spanwise Wall Oscillations'. In: *Applied Scientific Research* 55.4 (1996), pp. 311–326. ISSN: 0003-6994, 1573-1987. DOI: 10.1007/BF00856638.

[33] P. Baj, P. J. K. Bruce, and O. R. H. Buxton. 'The Triple Decomposition of a Fluctuating Velocity Field in a Multiscale Flow'. In: *Physics of Fluids* 27.7 (1st July 2015), p. 075104. ISSN: 1070-6631. DOI: 10.1063/1.4923744.

[34] Stephen B. Pope. 'Turbulent Flows'. In: *Measurement Science and Technology* 12.11 (Oct. 2001), pp. 2020–2021. ISSN: 0957-0233. DOI: 10.1088/0957-0233/12/11/705.

[35] J. Jeong and F. Hussain. 'On the Identification of a Vortex'. In: *Journal of Fluid Mechanics* 285 (Feb. 1995), pp. 69–94. ISSN: 1469-7645, 0022-1120. DOI: 10.1017/S0022112095000462.

[36] Kwing-So Choi, Timothy Jukes, and Richard Whalley. 'Turbulent Boundary-Layer Control with Plasma Actuators'. In: *Philosophical Transactions of the Royal Society A: Mathematical, Physical and Engineering Sciences* 369.1940 (13th Apr. 2011), pp. 1443–1458. DOI: 10.1098/rsta.2010.0362.

[37] F. Auteri et al. 'Experimental Assessment of Drag Reduction by Traveling Waves in a Turbulent Pipe Flow'. In: *Physics of Fluids* 22.11 (1st Nov. 2010), p. 115103. ISSN: 1070-6631. DOI: 10.1063/1.3491203.

[38] Maurizio Quadrio and Paolo Luchini. 'Method for Reducing the Viscous Friction between a Fluid and an Object'. Pat. WO2009000703A1 (WO). Politecnico Di Milano, Universita' Degli Studi Di Salerno. 31st Dec. 2008. URL: https://patents.google.com/patent/WO2009000703A1/en?oq=Patent+WO%2f2009%2f000703%2c+2008. (visited on 18/09/2021).

[39] Felix Kramer et al. 'Wavy Riblets for Turbulent Drag Reduction'. In: *5th Flow Control Conference*. 5th Flow Control Conference. Chicago, Illinois: American Institute of Aeronautics and Astronautics, 28th June 2010. ISBN: 978-1-62410-140-3. DOI: 10.2514/6.2010-4583.

[40] Rene Grüneberger et al. 'Influence of Wave-Like Riblets on Turbulent Friction Drag'. In: *Nature-Inspired Fluid Mechanics: Results of the DFG Priority Programme 1207 "Nature-Inspired Fluid Mechanics" 2006-2012*. Ed. by Cameron Tropea and Horst Bleckmann. Notes on Numerical Fluid Mechanics and Multidisciplinary Design. Berlin, Heidelberg: Springer, 2012, pp. 311–329. ISBN: 978-3-642-28302-4. DOI: 10.1007/978-3-642-28302-4_19.

[41] Sacha Ghebali, Sergei I. Chernyshenko, and Michael A. Leschziner. 'Can Large-Scale Oblique Undulations on a Solid Wall Reduce the Turbulent Drag?' In: *Physics of Fluids* 29.10 (1st Oct. 2017), p. 105102. ISSN: 1070-6631. DOI: 10.1063/1.5003617.

[42] Sacha Ghebali. 'Turbulent Drag Reduction by Oblique Wavy Wall Undulations'. PhD Thesis. Imperial College London, Apr. 2018. URL: http://spiral.imperial.ac.uk/handle/10044/1/63827 (visited on 18/09/2021).

[43] S. I. Chernyshenko and M. F. Baig. 'The Mechanism of Streak Formation in Near-Wall Turbulence'. In: *Journal of Fluid Mechanics* 544 (-1 18th Nov. 2005), p. 99. ISSN: 0022-1120, 1469-7645. DOI: 10.1017/S0022112005006506.

[44] M. van Nesselrooij et al. 'Drag Reduction by Means of Dimpled Surfaces in Turbulent Boundary Layers'. In: *Experiments in Fluids* 57.9 (Sept. 2016), p. 142. ISSN: 0723-4864, 1432-1114. DOI: 10.1007/s00348-016-2230-9.

[45] Davide Gatti and Maurizio Quadrio. 'Reynolds-Number Dependence of Turbulent Skin-Friction Drag Reduction Induced by Spanwise Forcing'. In: *Journal of Fluid Mechanics* 802 (Sept. 2016), pp. 553–582. ISSN: 0022-1120, 1469-7645. DOI: 10.1017/jfm.2016.485.

[46]   Kwing-So Choi. 'Near-Wall Structure of a Turbulent Boundary Layer with Riblets'. In: *Journal of Fluid Mechanics* 208 (Nov. 1989), pp. 417–458. ISSN: 1469-7645, 0022-1120. DOI: 10.1017/S0022112089002892.

[47]   P Luchini. 'Reducing the Turbulent Skin Friction'. In: *Computational Methods in Applied Sciences '96 (Paris, 9-13 September 1996)*. ECCOMAS Computational Fluid Dynamics Conference (3 ; Paris 1996-09-09) / ECCOMAS Conference on Numerical Methods in Engineering (2 ; Paris 1996-09-09). United Kingdom: John Wiley, Chichester, 1996, pp. 465–470. ISBN: 0-471-96226-0. URL: https://pascal-francis.inist.fr/vibad/index.php?action=getRecordDetail&idt=2723803 (visited on 06/09/2021).

[48]   Sergei Chernyshenko. 'Extension of QSQH Theory of Scale Interaction in Near-Wall Turbulence to All Velocity Components'. Version 2. In: *Journal of Fluid Mechanics* 916 (10th June 2021), A52. ISSN: 0022-1120, 1469-7645. DOI: 10.1017/jfm.2021.180. arXiv: 2002.05585.

[49]   Frank M. White. *Viscous Fluid Flow*. 2nd ed. McGraw-Hill Series in Mechanical Engineering. New York: McGraw-Hill, 1991. 614 pp. ISBN: 978-0-07-069712-6.

Appendix A

Code

"

Listing A.1: The following code is written in Python and is used to solve equations, as well as print figures.

```
import math
import numpy as np
import matplotlib
matplotlib.rcParams['text.usetex'] = True
import matplotlib.pyplot as plt
import sympy as sym
import scipy.integrate as integrate
from scipy.optimize import curve_fit
from scipy.optimize import fsolve


#import digitised data
ssl = np.genfromtxt('SSL.csv', delimiter=',')
ref = np.genfromtxt('reference.csv', delimiter=',')


#declare constants
r_m = 5.846
C_f0 = 0.0336*(360**(-.273))
Phi0inv = math.sqrt(C_f0/2)
k = 0.41
B = 5.0
diss_int = 0.3157
What = np.array([1, 2, 6, 12])
Psav_ssl_coeff = np.array([
    [1.135, 0.002929, -1.205E-6, 1.447E-10, -1.047E-13, 2.609E-17],
```

```python
    [-1.856, 0.03954, -5.2854E-5, 3.498E-8, -1.127E-11, 1.328E-15],
    [15.25, 0.04888, -4.441E-5, 1.628E-8, -2.845E-12, 1.938E-16],
    [27.90, 0.03824, -2.810E-5, 8.015E-9, -1.082E-12, 5.535E-17]
    ])


#function for curve fitting
def fit(x, a, b, c, q, r, p):
    return (x * (a*(x**2) + b*x + c)/(q*(x**2) + r*x + 1)) + p * (np.
        log(x+15)-np.log(15))


#symbolic fitted curve for sym.log if needed
def symfit(x, a, b, c, q, r, p):
    return (x * (a*(x**2) + b*x + c)/(q*(x**2) + r*x + 1)) + p * (sym.
        log(x+15)-sym.log(15))


#logarithmic profile
def loglaw(x, h):
    return (1/k) * np.log(x) + B + h


def symloglaw(x, h):
    return (1/k) * sym.log(x) + B + h


#for solving \overline{U}^{+}=y^{+} and logarithmic profile
def linlog(x, *h):
    return [loglaw(x[0], h) - x[1], x[0]-x[1]]


#declare figure
plt.figure(figsize=[5,3.75],dpi=246)


#separate arrays and plot digitised points of mean profile
x_ssl = ssl[:,0]
y_ssl = ssl[:,1]
plt.plot(x_ssl, y_ssl, mfc='none', mec='tab:orange',marker='o',
    markersize=6, linestyle='none', label='SSL')


x_ref = ref[:,0]
y_ref = ref[:,1]
plt.plot(x_ref, y_ref, mfc='none', mec='tab:blue',marker='^',
    markersize=6, linestyle='none', label='ref')
```

```python
#establish plotting linspace
xspace_ssl = np.linspace(0.5,109, num=250)
xspace_ref = np.linspace(0.5,198, num=600)


#curve fit and plot ssl and reference flow
popt_ssl, pcov_ssl = curve_fit(fit, x_ssl, y_ssl, maxfev = 5000)
plt.plot(xspace_ssl, fit(xspace_ssl, *popt_ssl), 'k-.', linewidth=1.5,
    label='SSL curve fit')


popt_ref, pcov_ref = curve_fit(fit, x_ref, y_ref, maxfev = 5000)
plt.plot(xspace_ref, fit(xspace_ref, *popt_ref), 'k--', linewidth=1.5,
    label='ref curve fit')


#plot \overline{U}^{+}=y^{+}
plt.plot(np.linspace(0.,30., num=50),np.linspace(0.,30., num=50),'k-',
    linewidth=1.5, label=r'$\overline{U}^+=y^+$')
plt.xlabel(r'$y^+$')
plt.ylabel(r'$\overline{U}^+$')


#plot graph
plt.legend(loc=4)
plt.grid()


#new graph for estimated log law
plt.figure(figsize=[5,3.75],dpi=246)
plt.plot(x_ssl, y_ssl, mfc='none', mec='tab:orange',marker='o',
    markersize=6, linestyle='none', label='SSL')
plt.plot(x_ref, y_ref, mfc='none', mec='tab:blue',marker='^',
    markersize=6, linestyle='none', label='ref')


#plot log law estimates
delh_ssl = 8
plt.plot(xspace_ssl, loglaw(xspace_ssl, delh_ssl), 'k-.', linewidth
    =1.5, label=r'SSL Log Profile')
plt.plot(xspace_ref, loglaw(xspace_ref, 0), 'k--', linewidth=1.5, label
    =r'Ref Log Profile')
plt.xlabel(r'$y^+$')
plt.ylabel(r'$\overline{U}^+$')
```

```python
#plot \overline{U}^{+}=y^{+}
plt.plot(np.linspace(0.,30., num=50),np.linspace(0.,30., num=50),'k-',
    linewidth=1.5, label=r'$\overline{U}^+=y^+$')
#plot graph
plt.legend(loc=4)
plt.grid()


#symbol for differentiation
x = sym.symbols('x')


#differentiate and square curve fits
diff_ssl = sym.diff(symfit(x, *popt_ssl),x)
diffsr_ssl = diff_ssl**2


diff_ref = sym.diff(symfit(x, *popt_ref),x)
diffsr_ref = diff_ref**2


#plot derivatives squared by lambdifying
diffsr_ssl_lm = sym.lambdify(x, diffsr_ssl, modules='numpy')
diffsr_ref_lm = sym.lambdify(x, diffsr_ref, modules='numpy')
plt.figure(figsize=[5,3.75],dpi=246)
plt.plot(xspace_ssl, diffsr_ssl_lm(xspace_ssl), 'k-.', label='SSL')
plt.plot(xspace_ref, diffsr_ref_lm(xspace_ref), 'k—', label='ref')
plt.grid()
plt.legend()
plt.xlabel(r'$y^+$')
plt.ylabel(r'$\left(\frac{d\overline{U}^+}{dy^+}\right)^2$')
max_range = 60
min_range = 0


#solve where log law estimate profile intersects u^+=y^+
ssl_cross = fsolve(linlog, [11,11], args=(delh_ssl))
ref_cross = fsolve(linlog, [11,11], args=(0))
#integrate estimate analytically
in_est_ssl = ssl_cross[0] + (1/(.41**2)) * (1/ssl_cross[0])
in_est_ref = ref_cross[0] + (1/(.41**2)) * (1/ref_cross[0])
print(ssl_cross[0],in_est_ssl,in_est_ref)
```

```python
#integrate curve fit numerically
in_ssl = integrate.quad(diffsr_ssl_lm, min_range, max_range)
in_ref = integrate.quad(diffsr_ref_lm, min_range, max_range)
print(in_ssl, in_ref)


#print out ratios for comparison
in_est_rat = in_est_ssl/in_est_ref
in_rat = in_ssl[0]/in_ref[0]
print(in_est_rat, in_rat, in_est_rat/in_rat)


in_est_rat = in_est_ssl/Phi0inv
in_rat = in_ssl[0]/Phi0inv
print(in_est_rat, in_rat, in_est_rat/in_rat)


#define functions to solve for P_{net,w}
def Psav_ssl(lm, coeff):
    a, b, c, d, e, f = coeff
    return a + b * lm + c * (lm**2)+ d * (lm**3) + e * (lm**4) + f * (
        lm**5)


def Preq_ssl(lm, i):
    return -100*diss_int*Phi0inv*(What[i]**2)\
            *((1-Psav_ssl(lm, Psav_ssl_coeff[i])/100)*2*math.pi/lm)
                **(1/3)


def Pnet_ww_ycross(ycross):
    return 100*(ycross-(1/k)*np.log(ycross)-B)*((2*C_f0)**(-1/2)+k/2)


def Psav_ww(ycross, tau_rat, lm, i):
    return 100*(Phi0inv*((((k*ycross)**2 + 1)/(ycross*(k**2)))*.9*(1-
        tau_rat/100)**(3/2)\
            -in_est_ssl*(1-Psav_ssl(lm, Psav_ssl_coeff[i])/100)))+
                Psav_ssl(lm, Psav_ssl_coeff[i])


def P_solve(z, *data):
    index, lmd = data
    Pnw = z[0]
    Psw = z[1]
```

```python
        ycr = z[2]
        return [Pnw-Psw-r_m*Preq_ssl(lmd, index),
                Pnw-Pnet_ww_ycross(ycr),
                Psw-Psav_ww(ycr, Pnw, lmd, index)]


#declare lambdas
lamb = np.linspace(250, 2500, num=2500)


#declare storage arrays
ycross_st = np.zeros((4, len(lamb)))
Pnet_ww_st = np.zeros((4, len(lamb)))
Psav_ww_st = np.zeros((4, len(lamb)))


#begin figure
plt.figure(figsize=[5,3.75],dpi=246)
#solve system and store
for i in range(4):
    for j in range(len(lamb)):
        Pnet_ww_st[i,j], Psav_ww_st[i,j], ycross_st[i,j] = fsolve(
            P_solve, [0,0,10], args=(i,lamb[j]))


#plot P_{net,w} as function of \lambda_{x}^{+0}
plt.plot(lamb, Pnet_ww_st[0], ls='-', label='%i ' % What[0])
plt.plot(lamb, Pnet_ww_st[1], ls='-.', label='%i ' % What[1])
plt.plot(lamb, Pnet_ww_st[2], ls=':', label='%i ' % What[2])
plt.plot(lamb, Pnet_ww_st[3], ls='--', label='%i ' % What[3])
plt.legend(title=r"$\hat{W}_\mathrm{s}^{+0}$")
plt.xlabel(r'$\lambda_{x}^{+0}$')
plt.ylabel(r'$P_\mathrm{net,w}$')
plt.grid()
plt.show()


#print y_{\times}^{+} and P_{net,w}
print(ycross_st)
print(Pnet_ww_st)
```